Pancreatic beta cell selective deletion of mitofusins 1 and 2 (*Mfn1* and *Mfn2*) disrupts mitochondrial architecture and abrogates glucose-stimulated insulin secretion *in vivo*

Eleni Georgiadou[1], Charanya Muralidharan[2], Michelle Martinez[2], Pauline Chabosseau[1], Alejandra Tomas[1], Fiona Yong Su Wern[3], Theodoros Stylianides[4], Stephen M. Rothery[5], Aida Di Gregorio[6], Isabelle Leclerc[1], Yusuf Ali[3], Amelia K. Linnemann[2], Tristan A. Rodriguez[6] and Guy A. Rutter[1,3*].

[1]Section of Cell Biology and Functional Genomics, Division of Diabetes, Endocrinology and Metabolism, Department of Medicine, Imperial College London, London, UK

[2]Center for Diabetes and Metabolic Diseases, Indiana University School of Medicine, Indianapolis, IN, USA

[3]Lee Kong Chian School of Medicine, Nanyang Technological University, Singapore

[4]Loughborough University, Centre of Innovative and Collaborative Construction Engineering, Leicestershire, UK

[5]FILM, Imperial College London, London, UK

[6]National Heart and Lung Institute, Imperial Centre for Translational and Experimental Medicine, Imperial College London, London, UK

Word count: 5492

*Address correspondence to Professor Guy A. Rutter, g.rutter@imperial.ac.uk, +44 20 759 43340

Abstract

Background and aims: Mitochondria are highly dynamic organelles, fundamental to cellular energy homeostasis. Mitochondrial metabolism of glucose is essential for the initiation of insulin release from pancreatic beta cells. Whether mitochondrial ultra-structure, and the proteins controlling fission and fusion, are important for glucose recognition are unclear. Mitochondrial fusion is supported by proteins including mitofusin 1 (MFN1), mitofusin 2 (MFN2) and optic atrophy (OPA1), and fission by dynamin-related protein 1 (DRP1). Here, we generated mice with beta cell-selective, adult-restricted deletion of *Mfn1* and *Mfn2* (β*Mfn1/2*-KO), and explored the impact on insulin secretion and glucose homeostasis *in vivo* and *in vitro.*

Materials and methods: C57BL/6J mice bearing *Mfn1* and *Mfn2* alleles with *lox*P sites, were crossed to animals carrying an inducible *Cre* recombinase at the Pdx1 locus (*Pdx*^{CreERT}). Isolated islets were used for live beta cell fluorescence imaging of cytosolic (Cal-520) or mitochondrial (Pericam) free Ca^{2+} concentration and membrane potential (TMRE). Mitochondrial network characteristics were quantified using super resolution fluorescence and transmission electron microscopy. Beta cell-beta cell connectivity was assessed using the Pearson (R) analysis and Monte Carlo simulation in intact mouse islets. Intravital imaging was performed in mice injected with an adeno-associated virus to express the cytosolic Ca^{2+} sensor GCaMP6s selectively in beta cells and TMRM to visualise mitochondria using multiphoton microscopy.

Results: β*Mfn1/2*-KO mice displayed higher fasting glycaemia than control littermates at 14 weeks (8.6 vs 6.4 mmol/L, $p>0.05$) and a >five-fold decrease in plasma insulin post-intraperitoneal glucose injection (5-15 min, $p<0.0001$). Mitochondrial length, and glucose-induced Ca^{2+} accumulation, mitochondrial hyperpolarisation and beta cell connectivity were all significantly reduced in β*Mfn1/2*-KO mouse islets. Examined by intravital imaging of the exteriorised pancreas, antiparallel changes in cytosolic Ca^{2+} and mitochondrial membrane potential, observed in control animals *in vivo*, were suppressed after *Mfn1/2* deletion.

Conclusion: Mitochondrial fusion and fission cycles are essential in the beta cell to maintain normal mitochondrial bioenergetics and glucose sensing both *in vitro* and in the living mouse. Such cycles may be disrupted in some forms of diabetes to impair mitochondrial function and, consequently, insulin secretion.

Keywords: Type 2 diabetes; pancreatic beta cell; mitochondrial dysfunction; mitofusins; GSIS.

Abbreviations

$[Ca^{2+}]_{cyt}$	Cytoplasmic Ca^{2+} concentration
$[Ca^{2+}]_{mito}$	Mitochondrial free Ca^{2+} concentration
β*Mfn1/2*-KO	Beta cell-specific Mfn1/2-null (animal)
$\Delta\psi_m$	Mitochondrial membrane potential
FCCP	Carbonyl cyanide-4-phenylhydrazone
GSIS	Glucose-stimulated insulin secretion
KO	Knockout
MFN	Mitofusin
MOI	Multiplicity of infection
mtDNA	mitochondrial DNA
NA	Numerical aperture
qRT-PCR	Quantitative RT-PCR
R	Pearson correlation coefficient
TMRE	Tetramethylrhodamine ethyl ester
TMRM	Tetramethylrhodamine methyl ester
WT	Wild-type

Introduction

Mitochondria are often referred to as the powerhouses, or more recently, as the "chief executive organelles" (CEO) of the cell, generating most of the energy required to sustain normal function. Mitochondria are responsible for nicotinamide adenine dinucleotide (NAD) and hydrogen (NADH) production via the Krebs cycle, oxidative phosphorylation, adenosine triphosphate (ATP) synthesis, fatty acid oxidation and gluconeogenesis, and mitochondrial DNA (mtDNA) distribution. They also contribute to the regulation of apoptosis and their own turnover via mitophagy [1].

Mitochondrial oxidative metabolism plays a pivotal role in the response of pancreatic beta cells to stimulation by glucose and other nutrients [2-4]. Thus, as concentrations of sugar increase in the blood, enhanced glycolytic flux and oxidative metabolism in these cells lead to an increase in ATP synthesis, initiating a cascade of events which involve the closure of ATP-sensitive K^+ (K_{ATP}) channels [5], plasma membrane depolarisation and the influx of Ca^{2+} via voltage-gated Ca^{2+} channels (VDCC). The latter mechanism, along with other, less well defined amplifying signals [6], drive the biphasic release of insulin [4].

The possibility that changes in mitochondrial function in these cells may contribute to declining insulin secretion and to type 2 diabetes (T2D) has been the subject of extensive investigation [7]. Reduced glucose-stimulated insulin secretion (GSIS) in beta cells, alongside altered mitochondrial function, dynamics and morphology, were observed in diabetic models [8-10].

Besides ATP, mitochondria are also one of the main producers of reactive oxygen species (ROS) in the cell, inducing oxidative stress and tissue damage [11]. Mitochondrial dysfunction in type 2 diabetic or obese patients suffering from hyperglycaemia was shown to be directly linked with over-production of ROS, lowered ATP levels and mitochondrial content as well as the development of insulin resistance [12]. Additionally, several mtDNA variations in human populations were associated with increased or decreased risk of T2D [13], while in animal models, alterations in beta cell mtDNA led to reduced insulin secretion, hyperglycemia and beta cell death [14].

The multifaceted roles of mitochondria in the cell are associated with an equally variable morphology. Under normal physiological conditions, these organelles repetitively undergo fusion and fission cycles which are essential for their quality control and adaptation to energetic demands [15]. Thus, highly inter-connected mitochondrial networks allow communication and interchange of contents between mitochondrial compartments, as well as with other organelles such as the endoplasmic reticulum (ER) [16]. These exist interchangeably with more fragmented structures, with the balance between the two influenced by external stimuli and metabolic demands [17]. Thus, in many cell types including INS1, a pro-fused state is often observed during starvation or acute oxidative stress where energy production is required for cytoprotection and resistance to apoptosis. The opposite pertains when cells are exposed to increased nutrient supply such as in obesity or T2D [18]. On the other hand, exposure to a nutrient overload can stimulate mitochondrial fission and uncoupled respiration [18], but is critical for the elimination of damaged mitochondria by mitophagy [19].

Over the past two decades, considerable light has been shed on the molecules and mechanisms that control mitochondrial dynamics. The mitofusins MFN1 and MFN2 are key mediators of mitochondrial outer membrane (OMM) fusion and OPA1 of the inner mitochondrial membrane (IMM) fusion, while DRP1 is responsible for mitochondrial fission [20].

In pancreatic beta cells, defects in mitochondrial structure, accumulation of damaged or depolarised organelles are associated with oxidative stress and the subsequent development of diabetes in patients and animal models [15]. Changes in mitochondrial fusion and fission dynamics are observed in the pancreatic beta cell in animal models of diabetes [7, 21, 22], and patients with T2D and obesity exhibited smaller and swollen mitochondria in pancreatic tissue samples [23]. The latter, was suggested to be a consequence of hyperglycemia [24], followed by increased ROS production demonstrating that mitochondrial dynamics can be master regulators of mitochondrial activity [25].

Suggesting that changes in the expression of mitochondrial fusion regulators may also be altered in diabetes in extra-pancreatic tissues, insulin resistant and obese patients show reduced *MFN2* expression in skeletal muscle [26]. Possibly resulting from altered expression of the peroxisome proliferator-activated receptor-gamma coactivator (PGC)-1alpha and the estrogen-related receptor alpha (ERRα) [27, 28]. This lead to increases in ROS production and impaired mitochondrial respiration in both skeletal muscle and liver tissues through the JNK pathway [27-29]. Whether these changes are the cause, or the consequence, of impaired mitochondrial dynamics, remains unclear, however [30-32].

To address this question in the context of the pancreatic beta cell, we explore the impact of targeted deletion of *Mfn1* and *Mfn2,* specifically in mouse beta cells in adult animals. We show that this exerts profound effects on beta cell mass, insulin secretion and glucose homeostasis.

Materials and Methods

Generation of beta cell-selective *Mfn1/Mfn2* knockout (β*Mfn1/2*-KO) mice C57BL/6J mice were housed in individually ventilated cages in a pathogen-free facility with a 10-14 h light-dark cycle and were fed *ad libitum* with a standard mouse chow diet (Research Diets). All *in vivo* procedures were approved by the UK Home Office, according to the Animals (Scientific Procedures) Act 1986 with local ethical committee approval under personal project license (PPL) number PA03F7F07 to I.L.

C57BL/6J male mice bearing *Mfn1* (Mfn1^{tm2Dcc}; JAX stock #026401) and *Mfn2* (B6.129(Cg)-Mfn2^{tm3Dcc}/J; JAX stock #026525) alleles [33] with *lox*P sites flanking exons 4 and 6 were purchased from the Jackson laboratory and crossed to C57BL/6J transgenic animals carrying an inducible *Cre* recombinase under *Pdx1* promoter control (Pdx-Cre^{ERT2}) [34]. Mice bearing floxed *Mfn* alleles but lacking *Cre* recombinase were used as wild-type (WT) littermate controls. Mice were genotyped following protocols described by the Jackson laboratory for each of these strains. (See ESM Table 1 for genotyping primer details). Recombination was achieved by daily tamoxifen (20mg/ml [diluted in corn oil; Sigma]) intraperitoneal (IP) injections for five days at 7-8 weeks of age. Body weight was monitored every week, for 14 weeks, in *ad libitum* fed mice.

mRNA extraction and quantitative reverse transcription PCR For measurements of mRNA levels, pancreatic islets from 14-week-old WT and β*Mfn1/2*-KO males were isolated by collagenase digestion. Gene expression was determined by quantitative reverse transcription PCR (qRT-PCR) and normalised to *β-actin* [35] (see ESM Table 2 for primer details).

IPGTT test and measurement of insulin secretion *in vivo* To investigate glucose tolerance, male mice (aged 14 weeks) were fasted overnight and injected with glucose (20% w/v, 1g/kg body weight) IP. Glucose was measured in tail vein blood at time points as indicated using an ACCU-CHECK Aviva glucometer (Roche). For *in vivo* insulin secretion measurements, fasted male mice were administered glucose (20% w/v, 3g/kg body weight) IP, and plasma insulin was measured using an ultra-sensitive mouse insulin enzyme-linked immunosorbent assay (ELISA) kit (CrystalChem).

***In vitro* insulin secretion** Insulin secretion assays were performed in triplicate on size-matched islets, isolated from male mice (14 weeks of age) and incubated for 1 h in Krebs-Ringer bicarbonate buffer (140 mmol/l NaCl, 3.6 mmol/l KCl, 0.5 mmol/l NaH_2PO_4, 2 mmol/l $NaHCO_3$ [saturated with CO_2], 1.5 mmol/l $CaCl_2$, 0.5 mmol/l $MgSO_4$, 10 mmol/l HEPES; pH 7.4) containing 3 mmol/l glucose. Subsequently, islets were incubated (10 islets/well) for 30 min in Krebs-Ringer solution with either 3 mmol/l, 17mmol/l glucose or 20mmol/l KCl. Secreted and total insulin content were quantified using a homogeneous time-resolved fluorescence (HTRF) insulin kit (Cisbio) in a PHERAstar reader (BMG Labtech), following the manufacturer's guidelines. Data are presented as secreted insulin/insulin content.

Single-cell fluorescence imaging Pancreatic islets were isolated from 14 or 20-week-old male mice, dissociated into single beta cells and plated onto glass coverslips [36]. To study mitochondrial structure, cells were incubated with 100nM Mitotracker green (Thermo Fischer) in Krebs-Ringer bicarbonate buffer containing 11 mmol/l glucose for 30 min. Mitotracker green was then washed with Krebs buffer with

11 mmol/l glucose before fluorescence imaging. Single channel image stacks for Mitotracker green were recorded on a LSM780 inverted confocal microscope (Carl Zeiss, Cambridge, UK) using a ×63 1.4 numerical aperture (NA) oil objective and excitation with an argon laser (488 nm) and captured using a GaAsP (Carl Zeiss) detector. The image X,Y and Z dimensions were optimised (Nyquist settings) prior to capture images to enable post processing by deconvolution using Huygens software (Scientific Volume Imaging).

For experiments with tetramethylrhodamine ethyl ester (TMRE), beta cells were loaded with 10 nmol/l TMRE in modified Krebs-Ringer bicarbonate buffer (140 mmol/l NaCl, 3.6 mmol/l KCl, 0.5 mmol/l NaH_2PO_4, 24 mmol/l NaHCO3 [saturated with CO_2], 1.5 mmol/l $CaCl_2$, 0.5 mmol/l $MgSO_4$, 10 mmol/l HEPES and 3 mmol/l glucose; pH 7.4) with 3 mmol/l glucose for 45 min and re-equilibrated with 2 nmol/l TMRE for 10 min before recordings. TMRE (2 nmol/l) was present throughout and fluorescence was excited at 550 nm. Carbonyl cyanide-4-phenylhydrazone (FCCP; 1 μmol/l) was administrated, as indicated, and imaging was performed using an AxioObserver.Z1 microscope (Zeiss) using a ×40 1.4 NA oil objective, a CMOS ORCA Flash 4 camera (Hamamatsu) and a Colibri.2 light emitting diode (LED) excitation system (Zeiss; excitation filter 534/20 nm; emission filter 572/28 nm) at 0.3 Hz (250 ms exposure). Data were analysed using ImageJ. Traces represent mean normalised fluorescence intensity over time (F/F_{min}), where F_{min} is the mean fluorescence recorded during the application of 3 mmol/l glucose.

Mitochondrial shape analysis To determine morphological characteristics of mitochondria, confocal stacks were analysed with ImageJ using an in-house macro

(available upon request). Briefly, for each stack, one image at the top, middle and bottom of the islet was analysed. After background subtraction, the following parameters were measured for each cell: number of particles, perimeter and circularity of each particle and elongation (1/circularity) was calculated [37]. The average perimeter, circularity and elongation of particles was then calculated for each cell.

Whole-islet fluorescence imaging Ca^{2+} imaging of whole islets was performed after infection with adenovirus encoding the mitochondrially-targeted probe, Pericam [36] (2mt8RP; multiplicity of infection [MOI]: 100; [48 h post-isolation]) in modified Krebs-Ringer bicarbonate buffer or incubation with cytosolic Cal-520 acetoxymethyl (AM; 2 μmol/l; 24 h post-isolation; Stratech) for 45 min in Krebs-Ringer bicarbonate buffer containing 3 mmol/l or 17 mmol/l glucose, 17 mmol/l glucose with 0.1 mmol/l diazoxide (Diaz; Sigma-Aldrich), or 20 mmol/l KCl with diazoxide. Images were captured at 0.5 Hz on a Zeiss Axiovert microscope equipped with a ×10 0.5 NA objective, a Hamamatsu image-EM camera coupled to a Nipkow spinning-disk head (Yokogawa CSU-10) and illuminated at 490 nm. Data were analysed using ImageJ.

Pancreas immunohistochemistry Isolated pancreata were fixed in 4% (vol/vol) buffered formalin and embedded in paraffin wax within 24 h of removal. Slides (5 μm) were submerged sequentially in Histoclear (Sigma, UK) followed by washing in decreasing concentrations of ethanol to remove paraffin wax. Permeabilised pancreatic slices were blotted with anti-guinea pig insulin (Agilent Technologies) and anti-mouse glucagon (1:1 000; Sigma) primary antibodies. Slides were visualised by subsequent incubation with Alexa Fluor 488 and 568-labelled donkey anti-guinea pig

and anti-mouse antibodies (1:1 000; Thermo Fischer). Samples were mounted on glass slides using Vectashield™ (Vector Laboratories) containing DAPI. Images were captured on a Zeiss AxioObserver.Z1 microscope using a ×40 Plan-Apochromat 206/0.8 M27 air objective, a CMOS ORCA Flash 4 camera (Hamamatsu) with a Colibri.2 LED illumination system (488 nm). Fluorescent quantification was achieved using Image J with a purpose-designed macro (available upon request). Whole pancreas was used to quantitate cell mass.

Electron microscopy (EM) For conventional EM, islets were chemically fixed in 2% paraformaldehyde (EM grade, TAAB Laboratories Equipment), 2% glutaraldehyde and 3 mM $CaCl_2$ in 0.1 M cacodylate buffer (Sigma) for 2 h at room temperature then left overnight at 4°C in fresh fixative solution, osmicated, enrobed in agarose plugs, dehydrated in ethanol and embedded on Epon (TAAB Laboratories Equipment). Epon was polymerised overnight at 60°C. Ultrathin 70 nm sections were cut with a diamond knife (DiATOME) in a Ultracut UCT ultramicrotome (Leica) before examination on a Tecnai T12 TEM (FEI). Images were acquired in a charge-coupled device camera (Eagle), and processed in ImageJ.

***In vivo* Ca^{2+} imaging of AAV8-INS-GCaMP6s infected endogenous pancreatic islets** All mice were IP injected with tamoxifen daily at 15 weeks old. Endogenous pancreatic islets of WT and β*Mfn1/2*-KO mice (16 weeks old) were then infected with AAV8-INS-GCaMP6s [38] viral particles ($10.1*10^{13}$ genome copies/ml) via IP injection (50μl/mouse), 24-28 days prior to terminal intravital imaging. On the day of imaging, mice were anesthetized with 2-4% inhaled isoflurane, the pancreas was then externalised and placed on a coverslip on a TCS SP8 DIVE (Leica) multiphoton

platform equipped with heating pads and an objective warmer. Heated blankets were used at all times and temperature was constantly monitored using a rodent rectal temperature probe throughout the imaging session. A ×40 1.1 NA water immersion objective was used during imaging. Islets were identified using green fluorescence from the GCaMP6s biosensor. Dyes suspended in saline, including Hoechst 33342 (Thermo Fisher Scientific: H3570; 70μg), tetramethylrhodamine methyl ester (TMRM, Thermo Fisher Scientific T668; 3μg) and Alexa Fluor 647 NHS Ester (Thermo Fisher Scientific; A20006) conjugated to Rat serum Albumin (Albumin-647; 500μg) were injected retro-orbitally to label nuclei, mitochondria and vasculature, respectively. *In vivo* Ca^{2+} imaging was performed by simultaneously exciting GCaMP6s at both 820 nm and 940 nm to capture non-excited and excited states of Ca^{2+} activity in the beta cells. Fluorescent emission was detected by an external HyD detector (Leica) through a 500-550 nm bandpass filter. Hoechst, TMRM and the dual excitable Albumin-647 were excited at 820 nm and fluorescence emission was detected by either external PMT (Leica) or HyD detectors through 400-470 nm, 570-630 nm and 650-750 nm bandpass filters, respectively. Baseline imaging of islets were recorded 10 min prior IP injection of glucose (1g/kg in sterile saline). The same islets were imaged for ~20 min to monitor Ca^{2+} oscillations post glucose injection. Baseline and post-imaging glucose measurements were obtained using an AlphaTRAK 2 glucometer. All images were collected at a scan speed of 600 Hz with a line average of 2, and a 512 x 512 frame size, with a frame rate of 0.576/s. At the end of each imaging session, animals were perfused with 4% (vol/vol) PFA and tissues were paraffin-embedded for further analysis. All *in vivo* imaging experiments were performed with approval and oversight from the Indiana University Institutional Animal Care and Use Committee (IACUC).

Fluorescent traces were calibrated to calculate fluorescence spikes fold change above the baseline on three cells per condition using ImageJ. Then the AUC was determined, with a threshold at 0.15 to subtract background noise.

Connectivity analysis

Pearson- R correlations. Significantly correlated beta cell pairs were measured on islets incubated with Cal-520 as described previously [39, 40]. Correlation coefficient (R) and heatmaps were generated using an in-house MATLAB script (available upon request).

Monte Carlo-based signal binarisation and data shuffling for identification of highly connected cells Data were analysed using approaches similar to those previously described [39, 40] with modifications as below. Ca^{2+} signals were denoised by subjecting the signal the Huang-Hilbert type (HHT) empirical mode decomposition (EMD). The signals were decomposed into their intrinsic mode functions (IMFs) in MATLAB [41]. The residual and the first IMF with the high-frequency components were then rejected to remove random noise.

The Hilbert-Huang Transform was then performed to retrieve the instantaneous frequencies [42-44] of the other IMFs to reconstruct the new signal using

$$X(t) = Re \sum_{j=1}^{N} a_j(t) e^{i \int \omega_j(t) dt}$$

where $a_j(t)$ = amplitude, $\omega_j(t)$ = frequency of the *i*th IMF component to retrieve a baseline trend and to account for any photobleaching or movement artefacts. A 20% threshold was imposed to minimise false positives from any residual fluctuations in baseline fluorescence.

Cells with deflection above the de-trended baseline were represented as '1' and inactivity represented as '0', thus binarising the signal at each time point. The coactivity of every cell pair was then measured as:

$$C_{ij} = \frac{T_{ij}}{\sqrt{T_i T_j}}$$

where T_{ij} = total coactivity time, T_i and T_j = total activity time for two cells.

The significance at $p<0.001$ of each coactivity measured against chance was assessed by subjecting the activity events of each cell to a Monte Carlo simulation [45, 46] with 10,000 iterations.

Synchronised Ca^{2+}-spiking behaviour was assessed by calculating the percentage of coactivity using the binarised cell activity dataset. A topographic representation of the connectivity was plotted in MATLAB with the edge colours representing the strength of the coactivity between any two cells.

An 80% threshold was imposed to determine the probability of the data, which was then plotted as a function of the number of connections for each cell to determine if the dataset obeyed a power-law relationship [47].

Statistical Analysis Data are expressed as mean ± SEM. Significance was tested by Student's two-tailed t-test, one or two-way ANOVA with Sidak's or Bonferroni multiple comparison test for comparison of more than two groups, using GraphPad Prism 8 software. $p<0.05$ was considered significant.

Results

Mfn1/2* ablation from pancreatic beta cells strongly inhibits GSIS *in vitro Deletion of *Mfn1* and *Mfn2* in islets was confirmed by qRT-PCR (Fig. **1A**). Relative to *β-actin*, expression of the *Mfn1* and *Mfn2* transcripts in islets from β*Mfn1/2*-KO mice decreased by ~83 and 86% accordingly vs control islets ($p<0.05$, $p<0.01$; Fig. **1A**). Body weight did not differ between groups over the first seven weeks post-tamoxifen injection (Fig. **1B**). Following this period, the mean body weight of β*Mfn1/2*-KO mice dropped significantly at 21-22 weeks ($p<0.05$), representing a 13% weight loss compared to the WT mice. We next explored the consequences of *Mfn1/2* deletion with regards to GSIS from isolated β*Mfn1/2*-KO islets at 14 weeks of age. With respect to WT controls, the latter displayed a sharply significant blunting in the secretory response to low and high glucose concentrations but also to depolarisation with KCl with near complete elimination of insulin secretion in response to stimulation ($p<0.05$; Fig. **1C**).

β*Mfn1/2*-KO mice are glucose intolerant with impaired GSIS *in vivo* To study the effects of mitofusin gene deletion in beta cells on systemic glucose homeostasis and insulin secretion *in vivo,* IP injections of 1g/kg body weight glucose (IPGTT) were performed on β*Mfn1/2*-KO and WT mice at 14 weeks of age (Fig. **2A**). The challenge revealed an impaired glucose tolerance in β*Mfn1/2*-KO mice compared to their control littermates with levels of glucose being higher at all time points following glucose injection (Fig. **2A-B**; $p<0.05$, $p<0.01$). Insulin concentrations were also measured following a 3g/kg body weight glucose IP injection (Fig. **2C-D**) during which, plasma was sampled at 0, 5, 15 and 30 min (Fig. **2E**). Basal glucose levels were modestly, but significantly higher in KO mice during all glucose challenges. β*Mfn1/2*-KO mice

showed dramatic lower insulin levels upon glucose challenge suggesting an insulin-secretory deficiency (Fig. **2E-F**, $p<0.05$, $p<0.001$, $p<0.0001$).

Deletion of *Mfn1/2* alters mitochondrial morphology in beta cells To assess changes in mitochondrial morphology, the mitochondria-targeted green fluorescence probe Mitotracker green was used. Deconvolved confocal images uncovered elongated mitochondria in dissociated WT beta cells at 14 weeks of age (Fig. **3A**). In contrast, the mitochondrial network in KO cells showed increased levels of fragmented organelles in absence of *Mfn1* and *Mfn2* (Fig. **3A**). Using ImageJ software to measure and quantify mitochondrial structural changes, results show that quantitation of the number of mitochondria per cell was not altered between groups (Fig. **3B**). Mitochondrial elongation and perimeter on the other hand, significantly decreased in β*Mfn1/2*-KO cells, representing rounder and smaller organelles (Fig. **3B**; $p<0.0001$). Mitochondrial clusters in KO cells had significantly higher circular shape as observed in the enlarged confocal images (Fig. **3B**; $p<0.0001$). Last, mitochondrial structure was evaluated in isolated islets by TEM and revealed highly fragmented mitochondria in KO mice compared to the WT group (Fig. **3C**). Cristae structure and organisation was also highly altered in β*Mfn1/2*-KO cells. More precisely, cristae invaginations were completely absent, as observed in the enlarged panels (Fig. **3C**).

***Mitofusins* are essential in maintaining normal glucose-stimulated Ca^{2+} uptake and mitochondrial membrane potential in beta cells** Since cytosolic Ca^{2+} is a major inducer of insulin exocytosis, Ca^{2+} dynamics in whole islets (14 weeks of age) were investigated by live-cell fluorescence microscopy in order to determine how

beta cell-specific *Mfn1/2* deletion in mitochondria might affect this pathway. Upon the perfusion of 17 mmol/l glucose, KO mouse islets pre-incubated with 3 mmol/l glucose, exhibited a significantly lower increase in cytosolic Ca^{2+} concentration ($[Ca^{2+}]_{cyt}$) compared to WT islets (AUC, $p<0.01$; Fig. **4A-B**). The K_{ATP} channel opener diazoxide and a depolarising K^+ concentration (20 mmol/l KCl) were then deployed together to bypass glucose regulation. Under these conditions, cytosolic Ca^{2+} increases were also impaired compared to WT animals (AUC, $p<0.01$; Fig. **4A-B**).

Since Ca^{2+} entry into the mitochondrial matrix is likely to be important for the stimulation of oxidative metabolism [48], we then determined the impact of deleting *Mfn1/2* on this process. Alterations in mitochondrial free Ca^{2+} concentration ($[Ca^{2+}]_{mito}$) were examined in whole islets infected with the mitochondrial Ca^{2+} sensor Pericam. Ablation of *Mfn1/2* strongly attenuated glucose-stimulated increases in $[Ca^{2+}]_{mito}$ in intact islets, where a substantial difference in response to 17 mmol/l glucose was observed between the two groups (Fig. **4C-D**). Additionally, glucose-induced increases in mitochondrial membrane potential ($\Delta\psi_m$), assessed with TMRE on 14 weeks dissociated beta cells, were abrogated in KO mice which were unable to sequester TMRE (AUC, $p<0.01$; Fig. **4E-F).** FCCP was used to induce depolarisation and completely eliminate $\Delta\psi_m$.

Beta cell-beta cell connectivity is impaired by *Mfn1/2* ablation Intercellular connectivity is required in the islet for a full insulin secretory response to glucose [10, 40]. To assess this, individual Ca^{2+} traces recorded from 14-weeks-Cal-520-loaded beta-cells in mouse islets (Fig. **4A**) were subjected to correlation (Pearson R) analysis to map cell-cell connectivity. Following perfusion at 17 mmol/l glucose,

β*Mfn1/2*-KO beta cells displayed an inferior, but not significantly different coordinated activity than WT cells (Fig. **5A**), as assessed by counting the number of coordinated cell pairs (Fig. **5C**; 0.94 vs 0.90 for WT vs KO, respectively). By contrast, beta cells displayed highly coordinated Ca^{2+} responses upon addition of 20 mM KCl (the latter stimulating depolarisation and a synchronised Ca^{2+} peak) in KO islets. Similarly, analysis of correlation strength in the same islets revealed significant differences in response to 17 mmol/l glucose between genotypes. In fact, KO islets had weaker mean beta-beta cell coordinated activity ($p<0.05$; Fig. **5B**, **D**; 0.88 vs 0.77 for WT vs KO, respectively), indicating that mitofusins affect the strength of connection rather than the number of coordinated beta cell pairs. We also explored beta cell connectivity using data binarisation and network theory to determine whether a hierarchy existed in the degree to which individual beta cells were coupled across the islet [39, 40]. Clear adherence to a power law distribution of connected beta cells was apparent in both islet groups in the elevated glucose condition (~10% of "hub" cells hosted >20% of all connections to other beta cells; R^2=0.21 for WT and R^2=0.45 for KO islets) (Supp. Fig. **1**). Thus, whilst lowering overall connectivity as assessed by either Pearson or Monte Carlo analysis, a similar proportion of cells served as hubs in each case.

***Mitofusin* deletion leads to beta cell loss** Immunohistochemical analysis in mice sacrificed at 14 weeks showed that deletion of *Mfn1* and *Mfn2* caused a gradual loss (~33%) of pancreatic beta (insulin-positive) cells in the KO group ($p<0.05$; Fig. **6A-B**). Alpha (glucagon-positive) cell surface was not affected by loss of mitofusin genes (Fig. **6C**). However, *Mfn1* and *Mfn2* loss was associated with a ~53% reduction in beta cell-alpha cell ratio ($p<0.05$; Fig. **6D**).

Glucose-induced cytosolic Ca^{2+} and $\Delta\psi_m$ changes are impaired in beta cells *in vivo* Two-photon imaging was adopted to allow visualisation of the intact pancreas, exposed through an abdominal incision on anaesthetised mice [49]. Islets previously infected *in vivo* with GCaMP6s and co-stained with TMRM immediately prior to data capture, were imaged for 18 min during which, cytosolic Ca^{2+} oscillations and mitochondrial membrane depolarisation were recorded post IP injection of glucose in WT (Fig. **7A**) and KO (Fig. **7B**) mice. Under these conditions, glucose concentrations in WT mice were 19 mmol/l and 33.3 mmol/l in KO animals after glucose injection. Analysis was performed on the most responsive beta cells where oscillations could be detected in both groups and revealed cytosolic Ca^{2+} oscillations (upward traces) and synchronous mitochondrial membrane depolarisation (downward traces; TMRM positive organelles) in response to elevated glucose in WT beta cells. On the other hand, cytosolic Ca^{2+} oscillations were largely abolished in β*Mfn1/2*-KO islets whilst fluctuations in TMRM fluorescence were still apparent in response to glucose (Fig. **7B**). Measurement of the area under the curve (AUC) of fold change traces above baseline depicted significantly impaired GCaMP6s spike signals in response to glucose ($p<0.05$; Fig. **7C**) and a tendency towards less TMRM uptake in β*Mfn1/2*-KO islets.

Discussion

Mitochondrial dynamics contribute to the maintenance of a metabolically-efficient mitochondrial population, with an impaired balance between fusion and fission impacting mitochondrial morphology and functionality. To date, dynamic and bioenergetic mitochondrial defects have been explored in conditional KO mouse models where different organs such as the liver, skeletal muscle, adipocyte, heart, nervous system, placenta and optic nerve were studied [50].

A number of studies have demonstrated that mitochondrial dysfunction contributes to the deterioration of beta cell function and plays a role in the development of T2D [3, 14, 51-53]. Deletion of *Drp1* from primary mouse beta cells resulted in glucose intolerant mice, with impaired GSIS and abnormal mitochondrial morphology associated with lower expression of MFN1, MFN2 and OPA1 [54, 55]. Similarly, over-expression of DRP1 in clonal INS1 cells decreased GSIS, increased ROS production and apoptosis [56] suggesting that a balance between fission and fusion is critical to avoid pathological changes. In line with these data, mice deficient for *Opa1* in the beta cell develop hyperglycemia, and show defects in ETC complex IV which lead to compromised glucose-stimulated ATP production, oxygen (O_2) consumption, Ca^{2+} dynamics, and insulin secretion [57].

In this study, we report that disturbance of the balance between fusion and fission leads to a profound disruption of beta cell function. Thus, using a novel mouse model to achieve highly efficient and selective ablation of *Mfn1* and *Mfn2* in pancreatic beta cells, we reveal that an intact mitochondrial network is essential to maintain normal insulin secretion and circulating glucose levels.

Deletion of *Mfn1/2*, ensured near-complete elimination of the mRNA encoding *Mfn1* and *Mfn2* throughout the beta cell population. As a consequence, β*Mfn1/2*-KO mice lost significant body weight, 14 weeks post tamoxifen injection, reflecting the characteristics of an ideal T2D model. In fact, and in agreement with previously–mentioned studies [3, 51-53], where altered mitochondrial dynamics affected beta cell function, GSIS post IP injection *in vivo* or in isolated islets *in vitro,* were severely compromised in our KO mouse model. Reduced insulin secretion capacity indicates that beta cells fail to respond to glucose, leading to impaired glucose clearance and hyperglycemia during IPGTTs. Higher fasting blood glucose levels were also characteristic of β*Mfn1/2*-KO mice suggesting that basal insulin secretion is inadequate to suppress hepatic glucose production.

We then assessed how mitochondrial morphology was affected in β*Mfn1/2*-KO beta cells, firstly by enhanced confocal microscopy. Deconvolved fluorescence images revealed distinct and more rounded organelles in the KO group while, WT littermates, had web-like mitochondria in dissociated beta cells, highlighting the specificity of the recombination system adopted. The higher degree of fragmentation was confirmed by quantifying organellar elongation, perimeter and circularity and could imply that other pro-fusion proteins might also be downregulated or, fission proteins are over-expressed. This could be confirmed by qRT-PCR and western blotting by studying the expression of OPA1, DRP1, FIS1 and other mitochondrial fusion/fission proteins. Last, the EM approach further confirmed mitochondrial fragmentation in isolated islets and interestingly, depicted disruptions in cristae shape and structure in KO mice. Mitochondrial adaptation to altered physiological conditions relies on the regulation of mitochondrial morphology, especially at the level of cristae compartment [58].

Changes in cristae number and shape delineate the respiratory capacity as well as cell viability [58]. Hence, altered assembly of IMM invaginations or even, loss of cristae may have a functional relevance to our animal model phenotype. Since cristae host the respiratory chain components, it is practical to hypothesise that more cristae translate into more respiratory capacity. An impaired cristae assembly could be synonymous with defective organisation of ETC complexes and lower ATP production, explaining the drop in insulin secretion observed *in vivo* and *in vitro*.

Under normal conditions, glucose-induced increases in cytosolic Ca^{2+} in insulin-producing beta cells stimulate insulin exocytosis by inducing closure of K_{ATP}-channels, plasma membrane depolarisation and Ca^{2+} influx via VDCC [4, 59]. Here, we demonstrate that this process is negatively affected in KO islets both *in vivo* and *in vitro* and speculate that this could be linked to less operational mitochondria, incapable of metabolising glucose and producing ATP. Since measurements of changes in $[Ca^{2+}]_{mito}$ performed in whole islets revealed a significant reduction in Ca^{2+} accumulation in these organelles, we can assume that mitochondrial dysfunction leads to impaired ATP production, lower cytosolic $[Ca^{2+}]$ and GSIS based on our own [60] and others' [61] previous work in beta cell lines and, very recently, with the generation of a beta cell-selective null mouse [35]. This is further endorsed by *in vivo* intravital imaging results, during which, cytosolic Ca^{2+} and $\Delta\psi_m$ traces along with fold change differences above baseline, uncovered less active beta cells in β*Mfn1/2*-KO islets in response to glucose. More precisely, in comparison to WT GCaMP6s infected beta cells where Ca^{2+} oscillations depicted cytosolic accumulation, β*Mfn1/2*-KO traces displayed failure to uptake Ca^{2+}. Additionally, TMRM imaging results indicated that KO mitochondria tended to be less depolarised than in WT islets. An observation that

correlates with TMRE fluorescence analysis performed on dissociated islets *in vitro,* where highly depolarised mitochondria were depicted in KO beta cells. On the other hand, WT beta cell mitochondria responded to increasing glucose concentrations with a corresponding increase in $\Delta\psi_m$, which correlated with an increase in insulin secretion [56]. It would also be interesting to investigate how ER homeostasis and Ca^{2+} storage and release are affected in KO cells since cytosolic and mitochondrial Ca^{2+} oscillations were deleteriously affected.

Interestingly, previous studies [62] have shown that inactivation of *Mfn*1 and *Mfn2* from the mouse heart leads to deficiencies in cardiac performance. Loss of beta cell identity is now thought to be a key element driving impaired beta cell function in T2D [4, 63] and may underlie impaired insulin secretion from remaining beta cells in type 1 diabetes [64]. As glucose-induced insulin secretion was almost eliminated *in vivo* and *in vitro* after *Mfn1/2* deletion in the beta cell, despite only partial loss of beta cells, our data support a similar change as contributing to functional alterations in the current model. Future studies, including measurements of the expression of key beta cell identity (and “disallowed”) [65] genes may be informative on this point.

Another finding of our study was that the strength of coordinated beta cell responses to 17 mmol/l glucose, using Pearson R analysis, was affected in β*Mfn1/2*-KO mice while no changes were identified in the number of glucose-responsive cells. This was also not associated with a loss of hierarchical behaviour and the loss of clearly identifiable “hub” cells following Monte Carlo simulation. Thus, we demonstrate that mitochondrial ultra-structure is important for normal beta-beta cell connections which

are, in turn, essential for coordinated Ca^{2+} influx into beta cells and ultimately, efficient and oscillatory insulin secretion [39].

Immunofluorescence analysis showed reduction in beta cell volume (the ratio of beta cell over total pancreas area) in KO islets describing the occurrence of beta cell loss and dysfunction in T2D [66]. This was additionally confirmed by a reduced yield and smaller size of islets isolated from β*Mfn1/2*-KO mice. The underlying mechanisms for the reduction of beta cell mass in β*Mfn1/2*-KO animals seems likely to be a dramatically increased rate of beta cell apoptosis [67] though we do not exclude altered beta cell replication or neogenesis [66] as contributors. Previous studies have raised a number of potential mechanisms by which mitochondrial fragmentation can affect apoptosis [68, 69]. Fragmentation occurs early in the cell death pathway [70] and is thought to contribute to cytochrome *c* production and release into the cytosol, and decrease in O_2 consumption, thereby enhancing oxidative stress and ROS production [71]. Future measurements of O_2 consumption rates and ROS production will be needed to explore these possibilities.

Other cellular signals have also been reported to induce a fragmented mitochondrial network by accelerating fission and inhibiting fusion [72]. These include extracellular signal-regulated protein kinases 1 and 2 (ERK1/2), known to inhibit fusion by phosphorylating DRP1 in cultured neuronal or tumour cells [72-74], while O-linked N-acetylglucosamine (O-GlcNAc) modifications, found to be elevated by high sugar, promoted OPA1 O-GlcNAcylation and impaired fusion in neonatal cardiomyocytes [75]. Whether post translation modifications of fusion proteins, including mitofusins,

are involved in settings of beta cell dysfunction in diabetes seems worthy of exploration.

In conclusion, we provide evidence that an altered balance of mitochondrial fusion and fission has a drastic impact on beta cell function. Our findings establish an important role for beta cell *Mfn1* and *Mfn2* in regulating plasma glucose levels, GSIS, islet Ca^{2+} oscillations and beta cell mass. Further investigation on the role of mitochondrial dynamics in insulin secretion, as well as, how changes in the expression of mitochondrial dynamics proteins could contribute to T2D would appear to be justified.

Conflict of Interest

G.A.R. received grant funding from Les Laboratoires Servier and was a consultant Sun Pharmaceuticals.

Acknowledgements We thank the Facility for Imaging by Light Microscopy (FILM) at Imperial College London for support with confocal and widefield microscopy image recording and analysis. We are also grateful to G. Carrat (Imperial College London) for generating the qRT-PCR primers.

Some of this work has been presented as an oral presentation at the Imperial College mitochondrial network, London, UK, February 2020, an oral presentation at the Diabetes UK Annual Professional Conference, Liverpool, UK, March 2019 and as a poster at the Gordon Research conference, Ventura, USA, March 2019.

Data availability All data generated or analysed during this study are included in the published article (and its supplementary information files). No applicable resources were generated or analysed during the current study.

Funding GAR was supported by a Wellcome Trust Senior Investigator Award (WT098424AIA) and Investigator Award (212625/Z/18/Z), MRC Programme grants (MR/R022259/1, MR/J0003042/1, MR/L020149/1), an Experimental Challenge Grant (DIVA, MR/L02036X/1), an MRC grant (MR/N00275X/1), and a Diabetes UK grant (BDA/11/0004210, BDA/15/0005275, BDA16/0005485). IL was supported by a Diabetes UK project grant (16/0005485). This project has received funding from the Innovative Medicines Initiative 2 Joint Undertaking, under grant agreement no. 115881 (RHAPSODY). This Joint Undertaking receives support from the European Union's Horizon 2020 research and innovation programme and EFPIA. This work is supported by the Swiss State Secretariat for Education, Research and Innovation (SERI), under contract no. 16.0097. AT was supported by MRC project grant MR/R010676/1. Intravital imaging was performed using resources and/or funding provided by National Institutes of Health grants R03 DK115990 (to AKL), Human Islet Research Network UC4 DK104162 (to AKL; RRID:SCR_014393).

Authors' relationships and activities GAR has received grant funding and consultancy fees from Les Laboratoires Servier and Sun Pharmaceuticals. The remaining authors declare that there are no relationships or activities that might bias, or be perceived to bias, their work.

Contribution statement EG performed experiments and analysed data. ATC performed the EM sample processing and data analysis. CM, MM and AKL were

responsible for the in vivo intravital Ca^{2+} imaging in mice. PC contributed to the analysis and manipulation of the *in vivo* intravital Ca^{2+} measurements. SMR supported the completion of confocal and widefield microscopy and analysis. TS contributed to the generation of the MATLAB script used for connectivity analysis. FYSW and YA generated and performed Monte Carlo-based signal binarisation. AR was involved in the design of the floxed *Mfn* alleles. TAR, ADG and IL were responsible for the maintenance and genotyping of mouse colonies and final approval of the version to be published. GAR designed the study and wrote the manuscript with EG with input and final approval of the version to be published from all authors. GAR is the guarantor of this work and, as such, had full access to all the data in the study and takes responsibility for the integrity of the data and the accuracy of the data analysis.

References

1. Chandhok, G., M. Lazarou, and B. Neumann, *Structure, function, and regulation of mitofusin-2 in health and disease.* Biol Rev Camb Philos Soc, 2018. **93**(2): p. 933-949.
2. Panten, U. and H. Ishida, *Proceedings: Flavin fluorescence of isolated pancreatic islets.* Naunyn Schmiedebergs Arch Pharmacol, 1974. **282**(Suppl): p. suppl 282:R73.
3. Maechler, P. and C.B. Wollheim, *Mitochondrial function in normal and diabetic beta-cells.* Nature, 2001. **414**(6865): p. 807-12.
4. Rutter, G.A., et al., *Pancreatic β-cell identity, glucose sensing and the control of insulin secretion.* Biochem J, 2015. **466**(2): p. 203-18.
5. Rorsman, P. and F.M. Ashcroft, *Pancreatic β-Cell Electrical Activity and Insulin Secretion: Of Mice and Men.* Physiol Rev, 2018. **98**(1): p. 117-214.
6. Henquin, J.C., *Triggering and amplifying pathways of regulation of insulin secretion by glucose.* Diabetes, 2000. **49**(11): p. 1751-60.
7. Supale, S., et al., *Mitochondrial dysfunction in pancreatic beta cells.* Trends Endocrinol Metab, 2012. **23**(9): p. 477-87.
8. Mulder, H. and C. Ling, *Mitochondrial dysfunction in pancreatic beta-cells in Type 2 diabetes.* Mol Cell Endocrinol, 2009. **297**(1-2): p. 34-40.
9. Del Guerra, S., et al., *Functional and molecular defects of pancreatic islets in human type 2 diabetes.* Diabetes, 2005. **54**(3): p. 727-35.
10. Rutter GA, et al., *Metabolic and functional specialisations of the pancreatic beta cell: gene disallowance, mitochondrial metabolism and intercellular connectivity.* Diabetologia under review, 2020.
11. Szendroedi, J., E. Phielix, and M. Roden, *The role of mitochondria in insulin resistance and type 2 diabetes mellitus.* Nature Reviews Endocrinology, 2012. **8**(2): p. 92-103.
12. Rovira-Llopis, S., et al., *Mitochondrial dynamics in type 2 diabetes: Pathophysiological implications.* Redox Biol, 2017. **11**: p. 637-645.
13. van den Ouweland, J.M., et al., *Functional and morphological abnormalities of mitochondria harbouring the tRNA(Leu)(UUR) mutation in mitochondrial DNA derived from patients with maternally inherited diabetes and deafness (MIDD) and progressive kidney disease.* Diabetologia, 1999. **42**(4): p. 485-92.
14. Haythorne, E., et al., *Diabetes causes marked inhibition of mitochondrial metabolism in pancreatic β-cells.* Nat Commun, 2019. **10**(1): p. 2474.
15. Wada, J. and A. Nakatsuka, *Mitochondrial Dynamics and Mitochondrial Dysfunction in Diabetes.* Acta Med Okayama, 2016. **70**(3): p. 151-8.
16. Rutter, G.A. and R. Rizzuto, *Regulation of mitochondrial metabolism by ER Ca2+ release: an intimate connection.* Trends in Biochemical Sciences, 2000. **25**(5): p. 215-221.
17. Westermann, B., *Bioenergetic role of mitochondrial fusion and fission.* Biochim Biophys Acta, 2012. **1817**(10): p. 1833-8.
18. Liesa, M. and O.S. Shirihai, *Mitochondrial dynamics in the regulation of nutrient utilization and energy expenditure.* Cell Metab, 2013. **17**(4): p. 491-506.
19. Wai, T. and T. Langer, *Mitochondrial Dynamics and Metabolic Regulation.* Trends Endocrinol Metab, 2016. **27**(2): p. 105-117.

20. *Mitochondrial Dynamics in Diabetes.* Antioxidants & Redox Signaling, 2011. **14**(3): p. 439-457.
21. Gao, Y., et al., *Evaluation of mitochondrial divisions in mouse with type-2 diabetes and effect of glucose-oxidase on mouse islet cells RIN-m5F.* Cell Biol Int, 2014. **38**(3): p. 368-73.
22. Higa, M., et al., *Troglitazone prevents mitochondrial alterations, beta cell destruction, and diabetes in obese prediabetic rats.* Proc Natl Acad Sci U S A, 1999. **96**(20): p. 11513-8.
23. Masini, M., et al., *Ultrastructural alterations of pancreatic beta cells in human diabetes mellitus.* Diabetes/Metabolism Research and Reviews, 2017. **33**(6): p. e2894.
24. Paltauf-Doburzynska, J., R. Malli, and W.F. Graier, *Hyperglycemic conditions affect shape and Ca2+ homeostasis of mitochondria in endothelial cells.* J Cardiovasc Pharmacol, 2004. **44**(4): p. 423-36.
25. Yu, T., J.L. Robotham, and Y. Yoon, *Increased production of reactive oxygen species in hyperglycemic conditions requires dynamic change of mitochondrial morphology.* Proc Natl Acad Sci U S A, 2006. **103**(8): p. 2653-8.
26. Zorzano, A., M. Liesa, and M. Palacin, *Mitochondrial dynamics as a bridge between mitochondrial dysfunction and insulin resistance.* Arch Physiol Biochem, 2009. **115**(1): p. 1-12.
27. Bach, D., et al., *Mitofusin-2 Determines Mitochondrial Network Architecture and Mitochondrial Metabolism: A NOVEL REGULATORY MECHANISM ALTERED IN OBESITY.* Journal of Biological Chemistry, 2003. **278**(19): p. 17190-17197.
28. Bach, D., et al., *Expression of Mfn2, the Charcot-Marie-Tooth neuropathy type 2A gene, in human skeletal muscle: effects of type 2 diabetes, obesity, weight loss, and the regulatory role of tumor necrosis factor alpha and interleukin-6.* Diabetes, 2005. **54**(9): p. 2685-93.
29. Schrepfer, E. and L. Scorrano, *Mitofusins, from Mitochondria to Metabolism.* Mol Cell, 2016. **61**(5): p. 683-694.
30. Quiros, P.M., et al., *Loss of mitochondrial protease OMA1 alters processing of the GTPase OPA1 and causes obesity and defective thermogenesis in mice.* Embo j, 2012. **31**(9): p. 2117-33.
31. Sebastian, D., et al., *Mitofusin 2 (Mfn2) links mitochondrial and endoplasmic reticulum function with insulin signaling and is essential for normal glucose homeostasis.* Proc Natl Acad Sci U S A, 2012. **109**(14): p. 5523-8.
32. Wang, L., et al., *Disruption of mitochondrial fission in the liver protects mice from diet-induced obesity and metabolic deterioration.* Diabetologia, 2015. **58**(10): p. 2371-80.
33. Chen, H., J.M. McCaffery, and D.C. Chan, *Mitochondrial fusion protects against neurodegeneration in the cerebellum.* Cell, 2007. **130**(3): p. 548-62.
34. Gu, G., J. Dubauskaite, and D.A. Melton, *Direct evidence for the pancreatic lineage: NGN3+ cells are islet progenitors and are distinct from duct progenitors.* Development, 2002. **129**(10): p. 2447-57.
35. Georgiadou E, et al., *The pore-forming subunit MCU of the mitochondrial Ca2+ uniporter is required for normal glucose-stimulated insulin secretion in vitro and in vivo in mice.* Diabetologia in press, 2020.
36. Tarasov, A.I., et al., *The Mitochondrial Ca2+ Uniporter MCU Is Essential for Glucose-Induced ATP Increases in Pancreatic β-Cells.* PLOS ONE, 2012. **7**(7): p. e39722.

37. Wiemerslage, L. and D. Lee, *Quantification of mitochondrial morphology in neurites of dopaminergic neurons using multiple parameters.* J Neurosci Methods, 2016. **262**: p. 56-65.
38. Reissaus, C.A., et al., *A Versatile, Portable Intravital Microscopy Platform for Studying Beta-cell Biology In Vivo.* Scientific Reports, 2019. **9**(1): p. 8449.
39. Salem, V., et al., *Leader β-cells coordinate Ca2+ dynamics across pancreatic islets in vivo.* Nature Metabolism, 2019. **1**(6): p. 615-629.
40. Johnston, N.R., et al., *Beta Cell Hubs Dictate Pancreatic Islet Responses to Glucose.* Cell Metab, 2016. **24**(3): p. 389-401.
41. Flandrin, G.R.a.P., *One or Two Frequencies? The Empirical Mode Decomposition Answers.* IEEE Transactions on signal processing, 2008. **56**(1).
42. Shen, N.E.H.a.S.S., *Hilbert–Huang Transform and Its Applications*, ed. I. Mathematical. Vol. 16. 2014.
43. Huang, N.E., *INTRODUCTION TO THE HILBERT–HUANG TRANSFORM AND ITS RELATED MATHEMATICAL PROBLEMS*, in *Hilbert-Huang Transform and Its Applications*. p. 1-26.
44. HUANG, N.E., et al., *ON INSTANTANEOUS FREQUENCY.* Advances in Adaptive Data Analysis, 2009. **01**(02): p. 177-229.
45. Shultis, W.D.a.J.K., *Exploring Monte Carlo Methods*. 1st ed, ed. E. Science. 2011. 398.
46. Björnsdotter, M., K. Rylander, and J. Wessberg, *A Monte Carlo method for locally multivariate brain mapping.* Neuroimage, 2011. **56**(2): p. 508-16.
47. Hodson, D.J., et al., *Investigating and modelling pituitary endocrine network function.* J Neuroendocrinol, 2010. **22**(12): p. 1217-25.
48. McCormack, J.G., A.P. Halestrap, and R.M. Denton, *Role of calcium ions in regulation of mammalian intramitochondrial metabolism.* Physiol Rev, 1990. **70**(2): p. 391-425.
49. Reissaus, C.A., et al., *A Versatile, Portable Intravital Microscopy Platform for Studying Beta-cell Biology In Vivo.* Sci Rep, 2019. **9**(1): p. 8449.
50. Eisner, V., M. Picard, and G. Hajnoczky, *Mitochondrial dynamics in adaptive and maladaptive cellular stress responses.* Nat Cell Biol, 2018. **20**(7): p. 755-765.
51. Lowell, B.B. and G.I. Shulman, *Mitochondrial dysfunction and type 2 diabetes.* Science, 2005. **307**(5708): p. 384-7.
52. Anello, M., et al., *Functional and morphological alterations of mitochondria in pancreatic beta cells from type 2 diabetic patients.* Diabetologia, 2005. **48**(2): p. 282-9.
53. Dlaskova, A., et al., *4Pi microscopy reveals an impaired three-dimensional mitochondrial network of pancreatic islet beta-cells, an experimental model of type-2 diabetes.* Biochim Biophys Acta, 2010. **1797**(6-7): p. 1327-41.
54. Reinhardt, F., et al., *Drp1 guarding of the mitochondrial network is important for glucose-stimulated insulin secretion in pancreatic beta cells.* Biochem Biophys Res Commun, 2016. **474**(4): p. 646-651.
55. Hennings, T.G., et al., *In Vivo Deletion of beta-Cell Drp1 Impairs Insulin Secretion Without Affecting Islet Oxygen Consumption.* Endocrinology, 2018. **159**(9): p. 3245-3256.
56. Stiles, L. and O.S. Shirihai, *Mitochondrial dynamics and morphology in beta-cells.* Best Pract Res Clin Endocrinol Metab, 2012. **26**(6): p. 725-38.

57. Zhang, Z., et al., *The dynamin-related GTPase Opa1 is required for glucose-stimulated ATP production in pancreatic beta cells.* Mol Biol Cell, 2011. **22**(13): p. 2235-45.
58. Quintana-Cabrera, R., et al., *Who and how in the regulation of mitochondrial cristae shape and function.* Biochemical and Biophysical Research Communications, 2018. **500**(1): p. 94-101.
59. Ashcroft, F.M. and P. Rorsman, *K(ATP) channels and islet hormone secretion: new insights and controversies.* Nat Rev Endocrinol, 2013. **9**(11): p. 660-9.
60. Tarasov, A.I., et al., *The mitochondrial Ca2+ uniporter MCU is essential for glucose-induced ATP increases in pancreatic beta-cells.* PLoS One, 2012. **7**(7): p. e39722.
61. Alam, M.R., et al., *Mitochondrial Ca2+ uptake 1 (MICU1) and mitochondrial ca2+ uniporter (MCU) contribute to metabolism-secretion coupling in clonal pancreatic β-cells.* J Biol Chem, 2012. **287**(41): p. 34445-54.
62. Song, M., et al., *Mitochondrial fission and fusion factors reciprocally orchestrate mitophagic culling in mouse hearts and cultured fibroblasts.* Cell Metab, 2015. **21**(2): p. 273-286.
63. Talchai, C., et al., *Pancreatic β cell dedifferentiation as a mechanism of diabetic β cell failure.* Cell, 2012. **150**(6): p. 1223-34.
64. Rui, J., et al., *β Cells that Resist Immunological Attack Develop during Progression of Autoimmune Diabetes in NOD Mice.* Cell Metab, 2017. **25**(3): p. 727-738.
65. Pullen, T.J., M.O. Huising, and G.A. Rutter, *Analysis of Purified Pancreatic Islet Beta and Alpha Cell Transcriptomes Reveals 11β-Hydroxysteroid Dehydrogenase (Hsd11b1) as a Novel Disallowed Gene.* Frontiers in Genetics, 2017. **8**(41).
66. Butler, A.E., et al., *Beta-cell deficit and increased beta-cell apoptosis in humans with type 2 diabetes.* Diabetes, 2003. **52**(1): p. 102-10.
67. Marchetti, P., et al., *Pancreatic islets from type 2 diabetic patients have functional defects and increased apoptosis that are ameliorated by metformin.* J Clin Endocrinol Metab, 2004. **89**(11): p. 5535-41.
68. Frank, S., et al., *The role of dynamin-related protein 1, a mediator of mitochondrial fission, in apoptosis.* Dev Cell, 2001. **1**(4): p. 515-25.
69. Olichon, A., et al., *Loss of OPA1 perturbates the mitochondrial inner membrane structure and integrity, leading to cytochrome c release and apoptosis.* J Biol Chem, 2003. **278**(10): p. 7743-6.
70. Heath-Engel, H.M. and G.C. Shore, *Mitochondrial membrane dynamics, cristae remodelling and apoptosis.* Biochim Biophys Acta, 2006. **1763**(5-6): p. 549-60.
71. Molina, A.J.A., et al., *Mitochondrial networking protects beta-cells from nutrient-induced apoptosis.* Diabetes, 2009. **58**(10): p. 2303-2315.
72. Sabouny, R. and T.E. Shutt, *Reciprocal Regulation of Mitochondrial Fission and Fusion.* Trends in Biochemical Sciences, 2020.
73. Prieto, J., et al., *Early ERK1/2 activation promotes DRP1-dependent mitochondrial fission necessary for cell reprogramming.* Nat Commun, 2016. **7**: p. 11124.
74. Kashatus, J.A., et al., *Erk2 phosphorylation of Drp1 promotes mitochondrial fission and MAPK-driven tumor growth.* Mol Cell, 2015. **57**(3): p. 537-51.

75. Hart, G.W., M.P. Housley, and C. Slawson, *Cycling of O-linked beta-N-acetylglucosamine on nucleocytoplasmic proteins.* Nature, 2007. **446**(7139): p. 1017-22.

Figure legends

Fig.1 Deletion of *Mfn1* and *Mfn2* from beta cells leads to body weight loss and impaired insulin secretion. (**A**) qRT-PCR quantification of *Mfn1* and *Mfn2* expression in islets relative to β-actin (*n*=3 mice per genotype in two independent experiments; 14 week-old-mice). (**B**) Measured body weight in WT (*Mfn1/2* $^{+/+}$) and β*Mfn1/2*-KO (*Mfn1/2* $^{-/-}$) mice (*n*=3-6 mice per genotype). (**C**) Insulin secretion from islets isolated from WT and KO mice during incubation of islets in 3 mmol/l glucose (3G), 17 mmol/l glucose (17G) or 20mmol/l KCl (*n*=4-5 mice per genotype; 14 week-old-mice). Blue, *Mfn1/2* $^{+/+}$ mice; red, *Mfn1/2* $^{-/-}$ mice. Data are presented as mean±SEM. *p<0.05; **p<0.01, analysed by unpaired two-tailed Student's t test.

Fig.2 β*Mfn1/2*-KO mice display highly impaired glucose tolerance *in vivo*. Glucose tolerance was measured in β*Mfn1/2*-KO mice and littermate controls (WT) by IPGTT (1 g/kg body weight) at (**A**) 14 weeks of age. (**B**) The corresponding AUC is shown for each graph (*n*=3-6 mice per genotype). (**C**) Glucose-induced insulin secretion (using 3 g/kg body weight) and (**D**) the corresponding AUC were assessed in 14-week-old β*Mfn1/2*-KO and WT mice (*n*=3-6 mice per genotype). (**E**) Plasma insulin levels during IPGTT in KO and WT mice (*n*=3-6 mice per genotype) and (**F**) the corresponding AUC. Blue, *Mfn1/2* $^{+/+}$ mice; red, *Mfn1/2* $^{-/-}$ mice. Data are presented as mean±SEM. *p<0.05; **p<0.01; ***p<0.001; ****p<0.0001 as indicated or WT vs KO mice at the time points indicated, analysed by unpaired two-tailed Student's t test or two-way ANOVA test.

Fig.3 Mitochondrial ultrastructure is altered following *Mfn1/2* deletion. (**A**) Confocal images of the mitochondrial network of dissociated beta cells (14 weeks of age) stained with Mitotracker green; scale bar: 5 μm. Lower right panels: magnification of selected areas. (**B**) Mitochondrial morphology analysis on deconvolved confocal images of dissociated beta cells. A macro was developed to quantify the number of mitochondria per cell and measure the elongation, perimeter and circularity (0: elongated; 1: circular mitochondria) of the organelles in WT and KO animals (*n*=3 mice per genotype). (**C**) Electron micrographs of mitochondria indicated with black thick arrows in islets isolated from *Mfn1/2* $^{+/+}$ and *Mfn1/2* $^{-/-}$ mice; scale bars: 1μm. Right panel: magnification of selected areas showing the cristae structure (black

arrow head); scale bar: 0.5 μm. Blue, *Mfn1/2* $^{+/+}$ mice; red, *Mfn1/2* $^{-/-}$ mice. Data are presented as mean±SEM. ****p<0.0001 as indicated, analysed by unpaired two-tailed Student's t test.

Fig.4 *Mfn1/2* deletion from pancreatic beta cells impairs cytosolic and mitochondrial Ca^{2+} uptake and changes in mitochondrial potential *in vitro*. (**A**) $[Ca^{2+}]_{cyt}$ changes in response to 17 mmol/l glucose (17G; with or without diazoxide [diaz]) or 20 mmol/l KCl with diaz were assessed following Cal-520 uptake in whole islets (14 weeks of age). Traces represent mean normalised fluorescence intensity over time (F/F_{min}). 3G, 3 mmol/l glucose. (**B**) The corresponding AUC is also presented (*n*=4 mice per genotype; 17G AUC measured between 245 s and 1045 s, 17G+diaz AUC measured between 1046 s and 1330 s), and KCl+diaz AUC measured between 1331 s and 1500 s). (**C**) $[Ca^{2+}]_{mito}$ changes in response to 17G and 20 mmol/l KCl were assessed in 20 weeks of age islets following Pericam infection. Traces represent mean normalised fluorescence intensity over time (F/F_{min}). (**D**) The corresponding AUC is also shown (n=2 mice per genotype; 17G AUC measured between 300 s and 1200 s, and KCl AUC measured between 1201 s and1500 s). (**E**) Dissociated beta cells (14 weeks of age) were loaded with TMRE to measure changes in $\Delta\psi_m$, and perifused with 3 mmol/l glucose (3G), 17G or FCCP as indicated. Traces represent normalised fluorescence intensity over time (F/Fmin). (**F**) AUC between 700–730 s (under 17G exposure) was determined from the data shown in (**E**) and presented as mean±SEM (data points from n=3-6 mice per genotype. Blue, *Mfn1/2* $^{+/+}$ mice; red, *Mfn1/2* $^{-/-}$ mice. Data are presented as mean±SEM. **p<0.01, assessed by unpaired two-tailed Student's t test or two-way ANOVA test.

Fig.5 Impact of *Mfn1/2* deletion on intercellular connectivity. (**A**) Representative cartesian maps of islets with colour coded lines connecting cells according to the strength of Pearson analysis (colour coded R values from 0 to 1, blue to red respectively) under 3mmol/l (3G), 17mmol/l (17G) glucose or 20mmol/l KCl; scale bars: 40 μm. (**B**) Representative heatmaps depicting connectivity strength (Pearson correlation coefficient (R)) of all cell pairs according to the colour coded R values from 0 to 1, blue to yellow respectively. (**C**) Percentage of correlated cell pairs at 3G, 17G or KCl (*n* = 4 mice per genotype). (**D**) Correlation coefficient values between

beta cells in response to glucose or KCl (*n* =4 mice per genotype). Blue, *Mfn1/2* $^{+/+}$ mice; red, *Mfn1/2* $^{-/-}$ mice. Islets were isolated from 14-week-old mice. Data are presented as mean±SEM. *p<0.05, assessed by two-way ANOVA test.

Fig.6 Absence of *Mfn1/2* in beta cells leads to decreased beta cell mass. (**A**) Representative pancreatic sections immunostained with glucagon (red) and insulin (green); scale bars: 30-50μm. (**B**) The beta cell and alpha cell surface (**C**) measured within the whole pancreatic area in WT and KO mice were determined, as well as the beta/alpha cell ratio in (**D**), (*n*=4 mice per genotype; experiment performed in triplicate). Blue, *Mfn1/2* $^{+/+}$ mice; red, *Mfn1/2* $^{-/-}$ mice. Islets were isolated from 14-week-old mice. Data are presented as mean±SEM. *p<0.05, assessed by unpaired two-tailed Student's t test.

Fig.7 Deletion of Mfn1/2 impairs beta cell function *in vivo***.** Representative image showing GCaMP6s labelled islets and TMRM stained mitochondria surrounded by the vasculature *in vivo* in WT and β*Mfn1/2*-KO mice. (**A**) Traces depicting fluorescence intensity of cytosolic Ca^{2+} (GCaMP6s) and mitochondrial TMRM signals in WT and (**B**) KO animals; scale bar: 45 μm; (*n* = 2 animals per genotype). Parallel and anti-parallel fluorescent signals are shown within selected areas. (C) AUC of fold change measurements above baseline for each GCaMP6s and TMRM traces measured (*n*= 3 cells per islet). Green, GCaMP6s; red, TMRM signals. Islets were imaged in 20-week-old mice. Data are presented as mean±SEM. *p<0.05, assessed by two-way ANOVA test.

Supplemental Fig.1 Mapping of beta cell population dynamics. (**A**) Representative cartesian maps of 14 week old islets stained with Cal-520 with colour coded lines connecting cells according to the strength of Pearson analysis (colour coded R values from 0 to 1, blue to red respectively) under 3mmol/l (3G), 17mmol/l (17G) glucose or 20mmol/l KCl (**B**) Log-log graph of the beta cell-beta cell connectivity distribution at 17 mmol/l glucose. WT and KO beta cells display obedience to a power-law distribution whereby few beta cells host at least, 20% of the connections to the rest of the beta cell population (*n*= 1 animal per genotype).

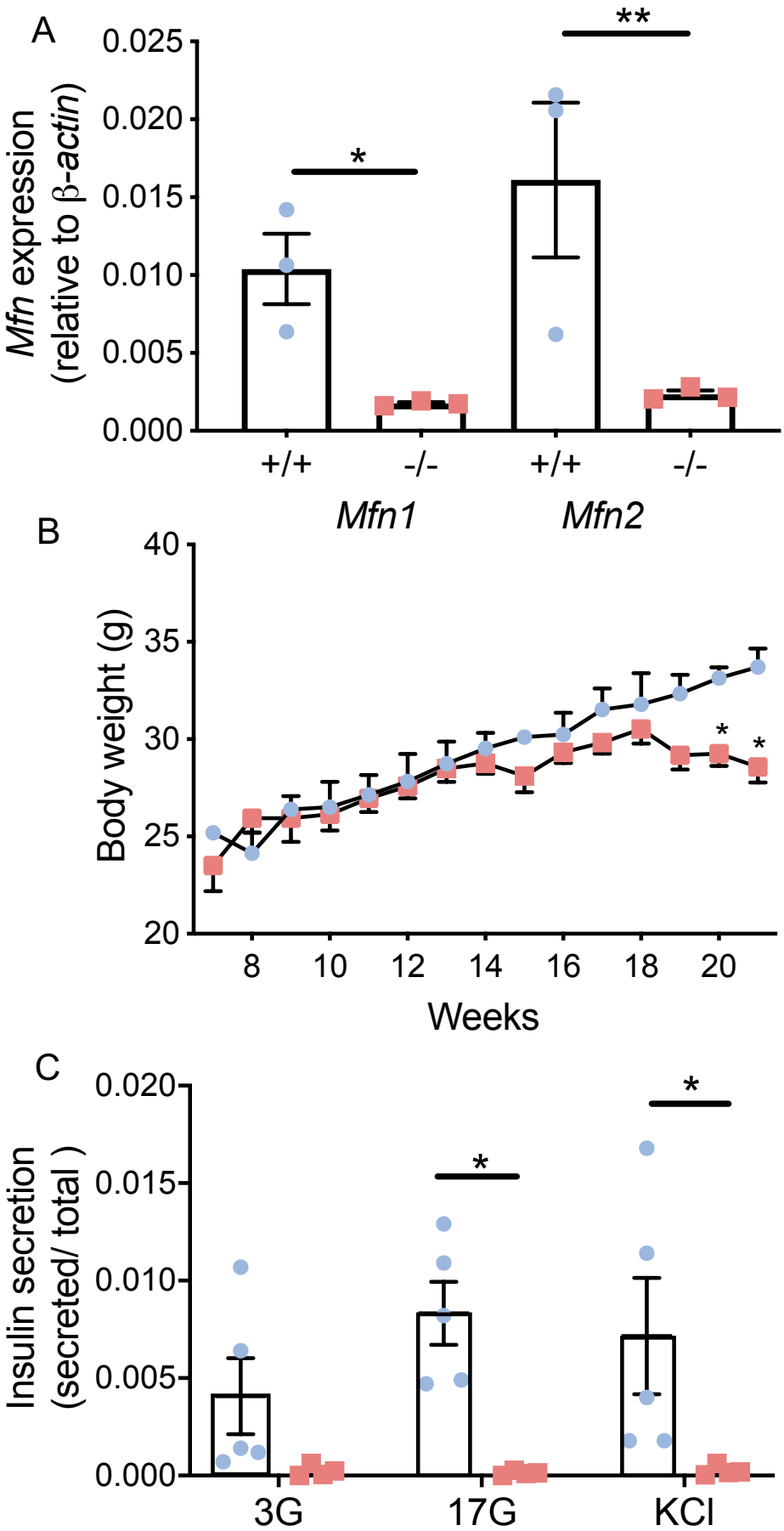
A
0.025
0.020
0.015
0.010
0.005
0.000
Mfn expression
(relative to β-actin)
*
**
+/+
-/-
+/+
-/-
Mfn1
Mfn2
B
40
35
30
25
20
Body weight (g)
*
*
8
10
12
14
16
18
20
Weeks
C
0.020
0.015
0.010
0.005
0.000
Insulin secretion
(secreted/ total)
*
*
3G
17G
KCl

Fig.1

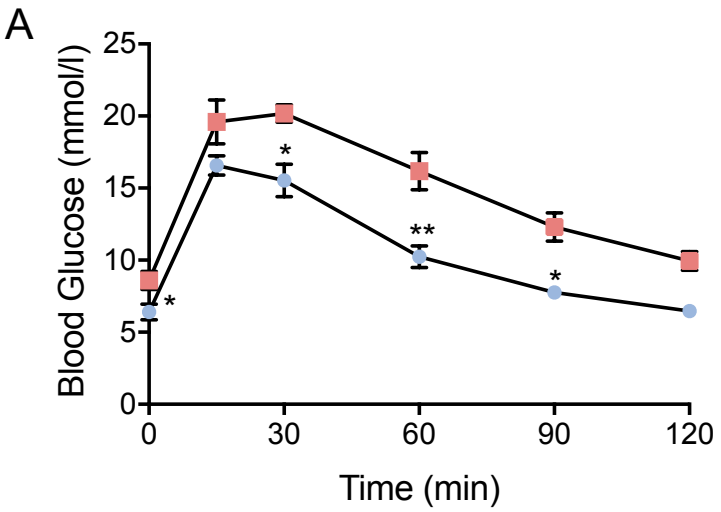
A
Blood Glucose (mmol/l)
25
20
15
10
5
0
0
30
60
90
120
Time (min)
*
*
**
*

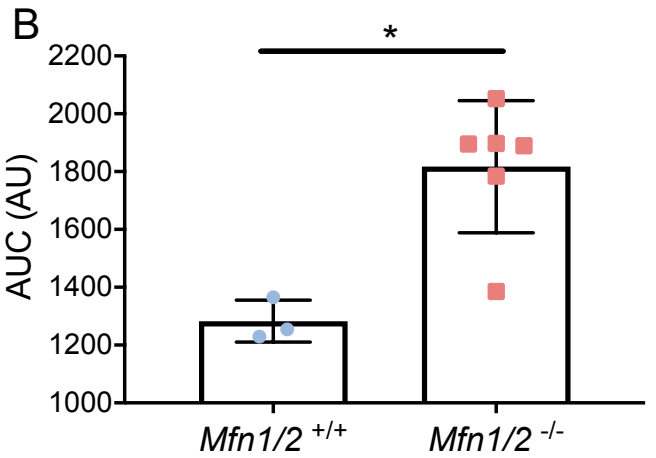
B
AUC (AU)
2200
2000
1800
1600
1400
1200
1000
*
Mfn1/2 +/+
Mfn1/2 -/-

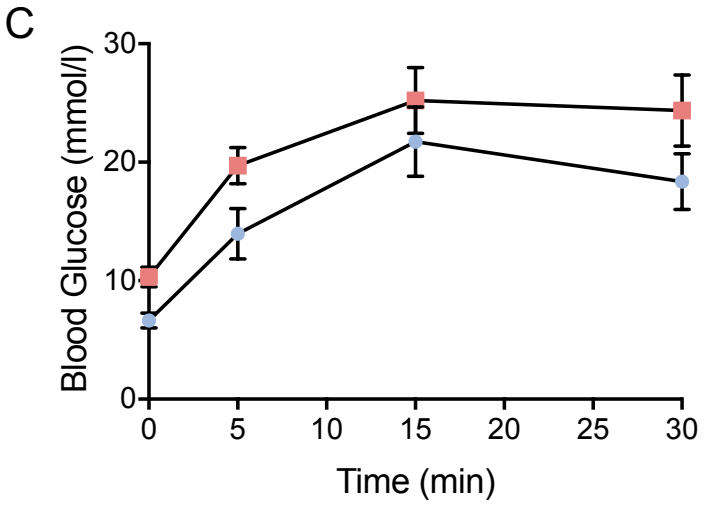
C
Blood Glucose (mmol/l)
30
20
10
0
0
5
10
15
20
25
30
Time (min)

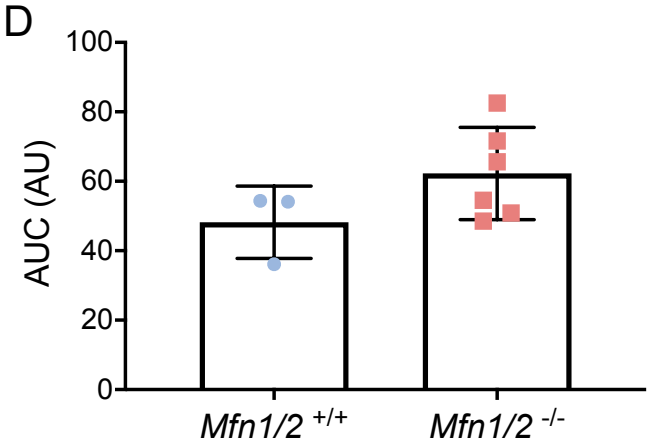
D
AUC (AU)
100
80
60
40
20
0
Mfn1/2 +/+
Mfn1/2 -/-

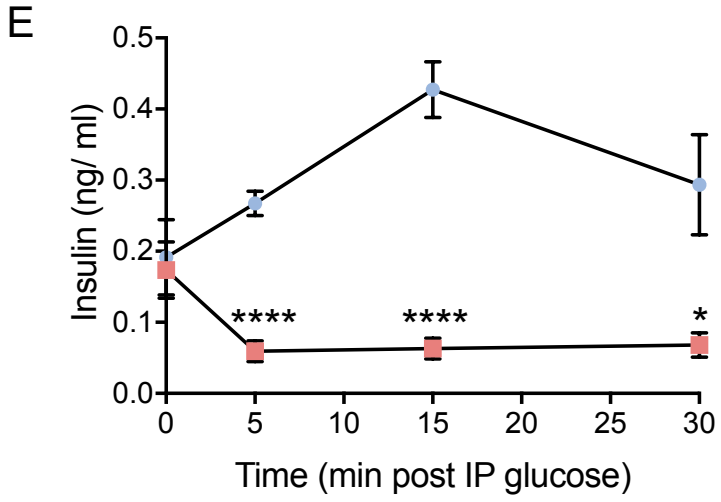
E
Insulin (ng/ ml)
0.5
0.4
0.3
0.2
0.1
0.0
0
5
10
15
20
25
30
Time (min post IP glucose)
****
****
*

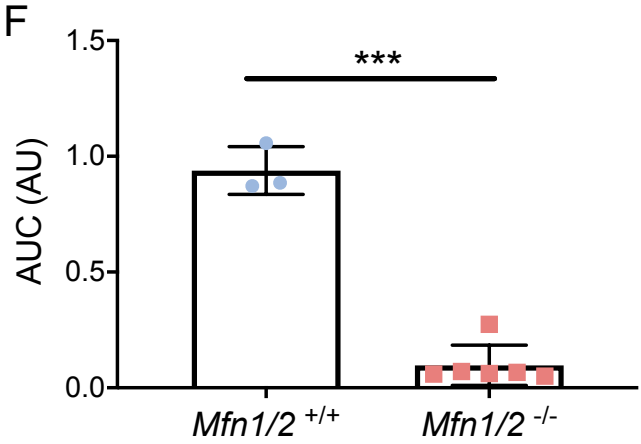
F
AUC (AU)
1.5
1.0
0.5
0.0
***
Mfn1/2 +/+
Mfn1/2 -/-

Fig.2

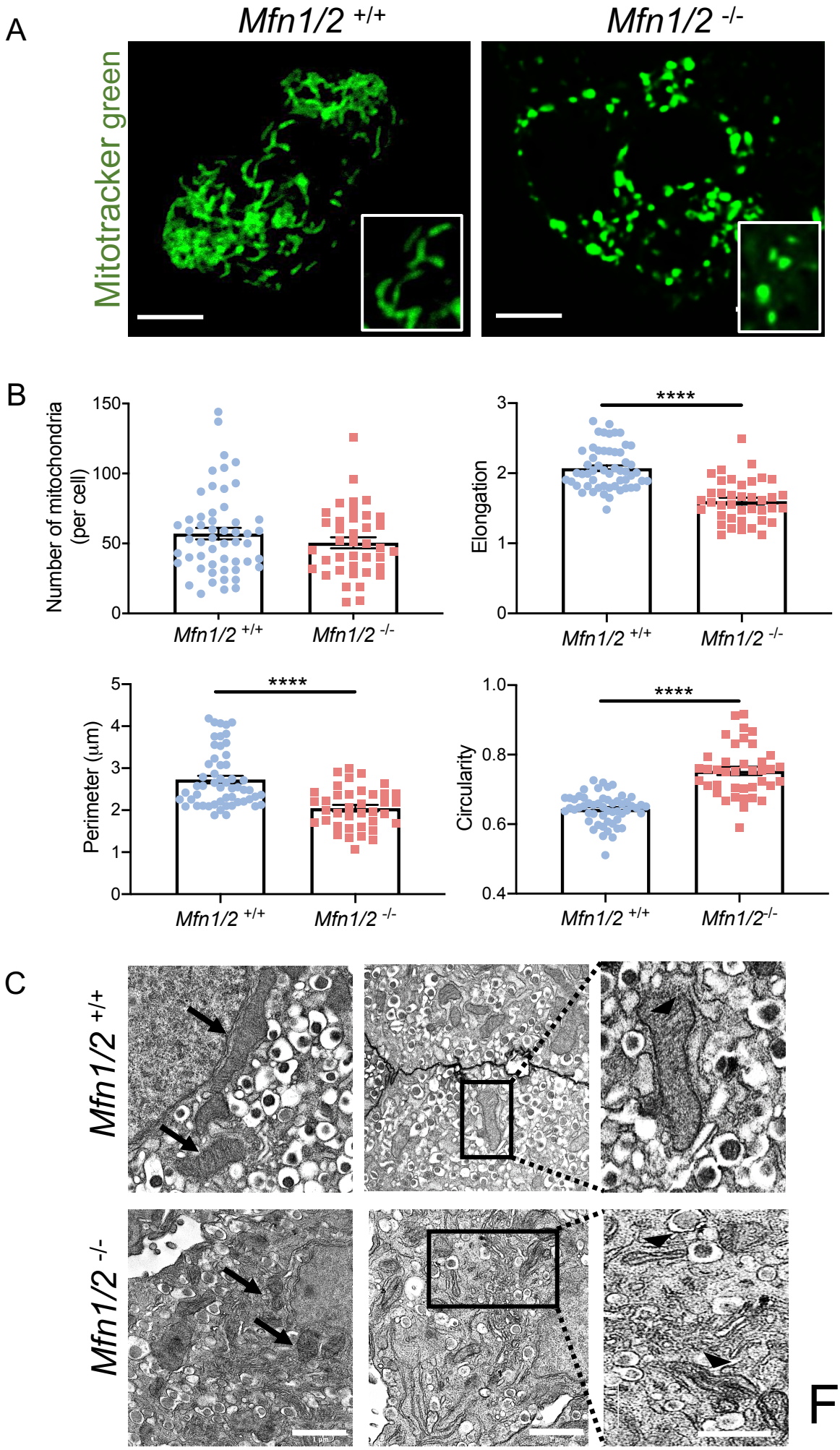
A
Mfn1/2 +/+
Mfn1/2 -/-
Mitotracker green
B
Number of mitochondria (per cell)
150
100
50
0
Mfn1/2 +/+
Mfn1/2 -/-
Elongation
3
2
1
0
****
Perimeter (μm)
5
4
3
2
1
0
****
Circularity
1.0
0.8
0.6
0.4
****
C
Mfn1/2 +/+
Mfn1/2 -/-

Fig.3

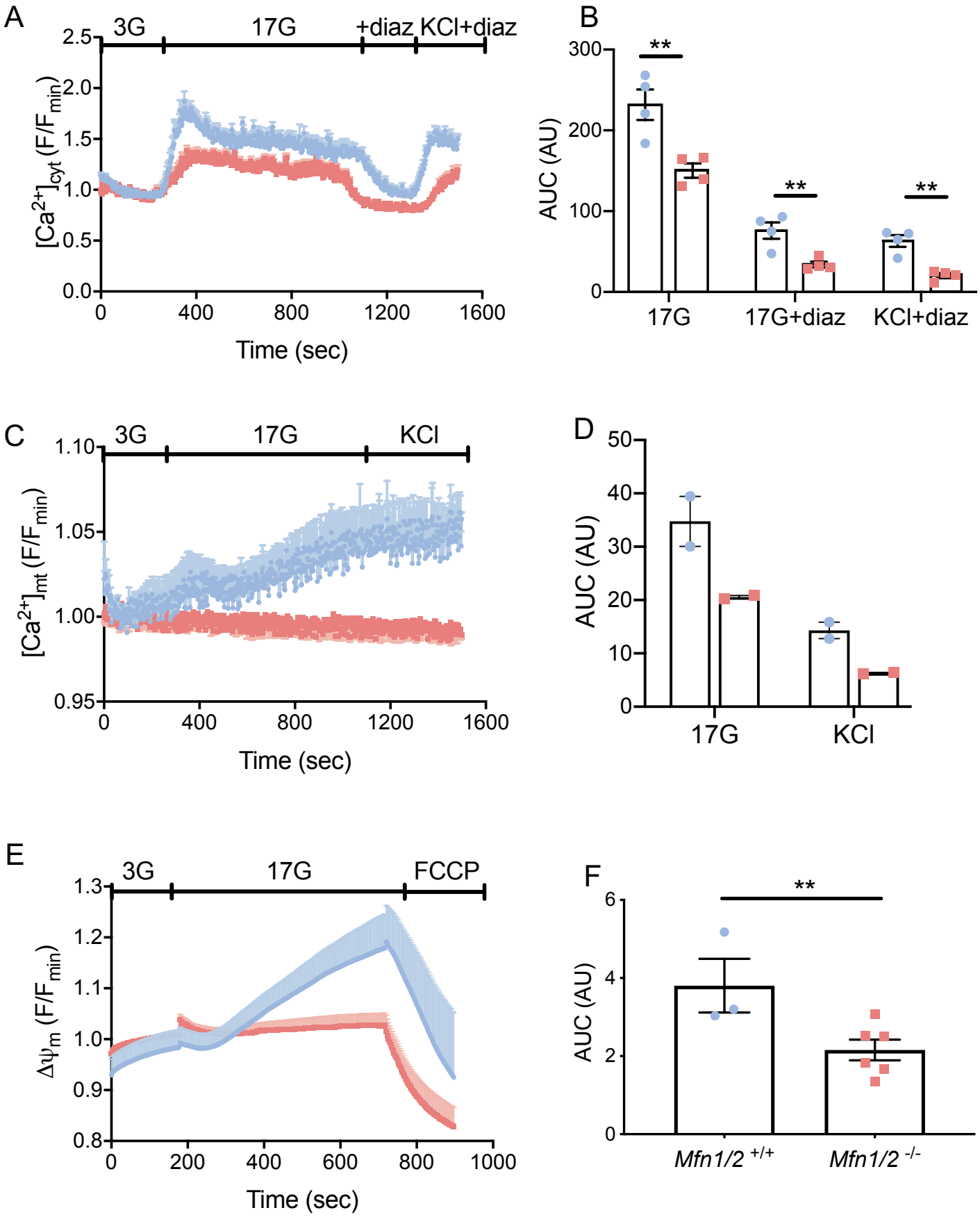
A
3G
17G
+diaz
KCl+diaz
$[Ca^{2+}]_{cyt}$ (F/F$_{min}$)
Time (sec)
B
AUC (AU)
**
17G
17G+diaz
KCl+diaz
C
3G
17G
KCl
$[Ca^{2+}]_{mt}$ (F/F$_{min}$)
Time (sec)
D
AUC (AU)
17G
KCl
E
3G
17G
FCCP
$\Delta\psi_m$ (F/F$_{min}$)
Time (sec)
F
AUC (AU)
**
Mfn1/2 $^{+/+}$
Mfn1/2 $^{-/-}$

Fig.4

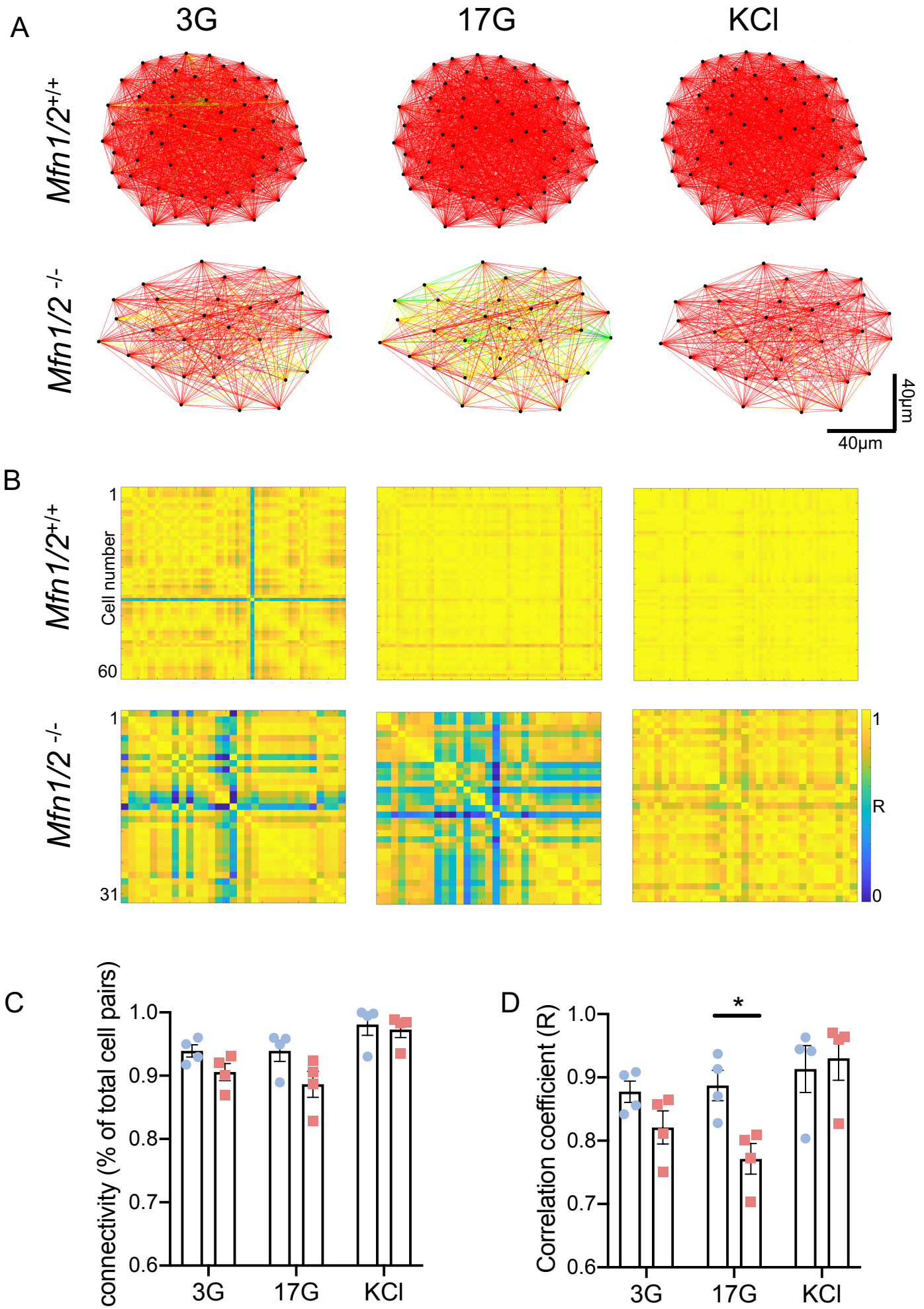
A
3G
17G
KCl
Mfn1/2+/+
Mfn1/2 -/-
40μm
40μm
B
Mfn1/2+/+
Mfn1/2 -/-
Cell number
1
60
1
31
1
R
0
C
connectivity (% of total cell pairs)
1.0
0.9
0.8
0.7
0.6
3G
17G
KCl
D
Correlation coefficient (R)
*
1.0
0.9
0.8
0.7
0.6
3G
17G
KCl

Fig.5

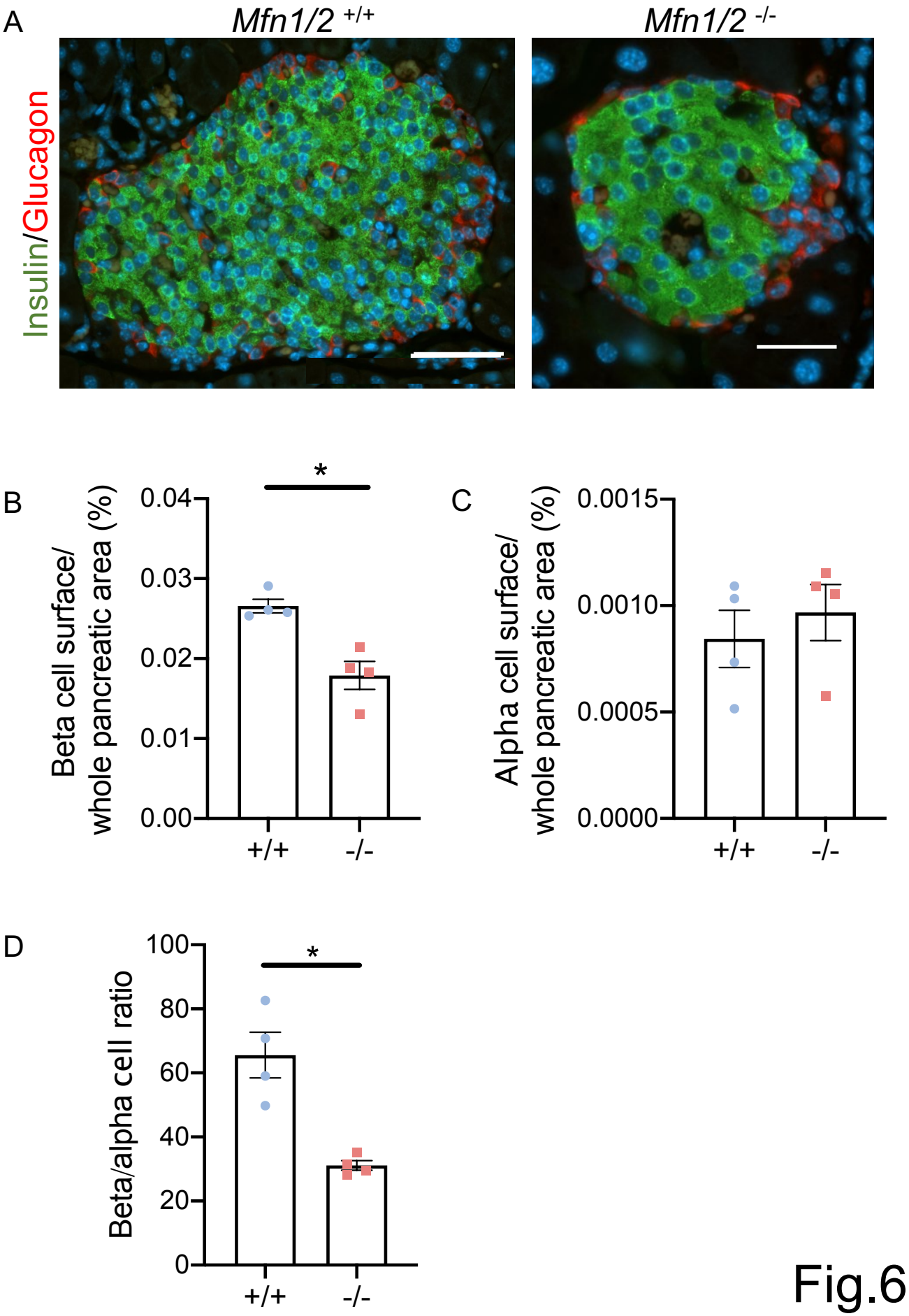
A
Mfn1/2 +/+
Mfn1/2 -/-
Insulin/Glucagon
B
Beta cell surface/
whole pancreatic area (%)
0.04
0.03
0.02
0.01
0.00
*
+/+
-/-
C
Alpha cell surface/
whole pancreatic area (%)
0.0015
0.0010
0.0005
0.0000
+/+
-/-
D
Beta/alpha cell ratio
100
80
60
40
20
0
*
+/+
-/-

Fig.6

A

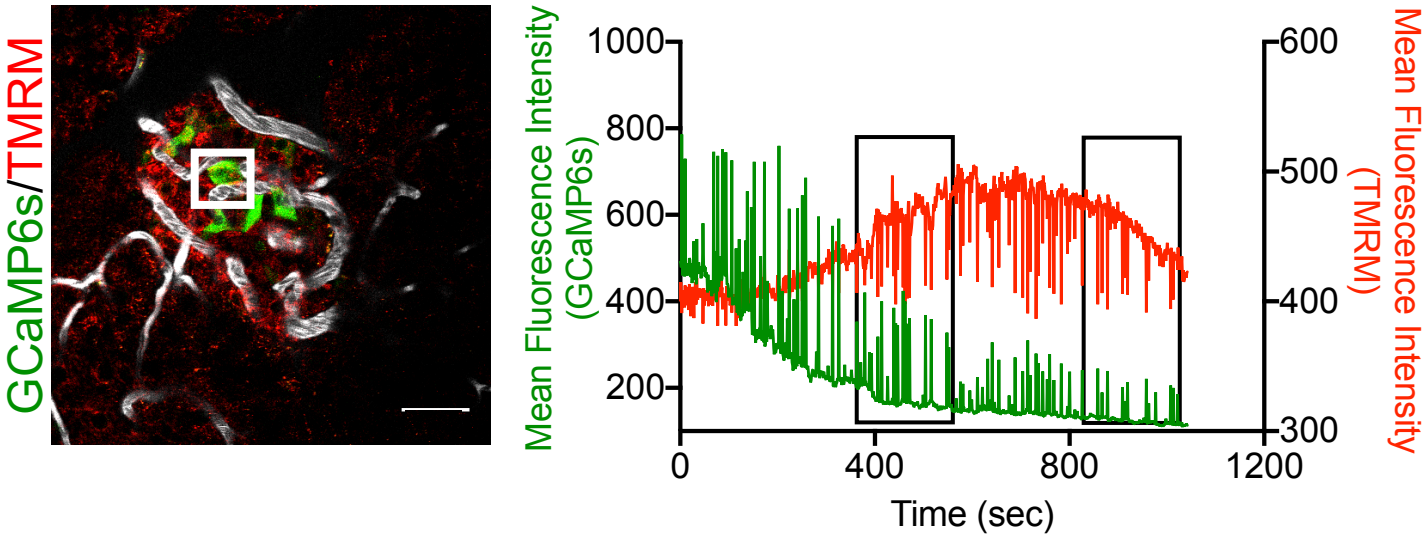
GCaMP6s/TMRM
Mean Fluorescence Intensity (GCaMP6s)
1000
800
600
400
200
Mean Fluorescence Intensity (TMRM)
600
500
400
300
0
400
800
1200
Time (sec)

B

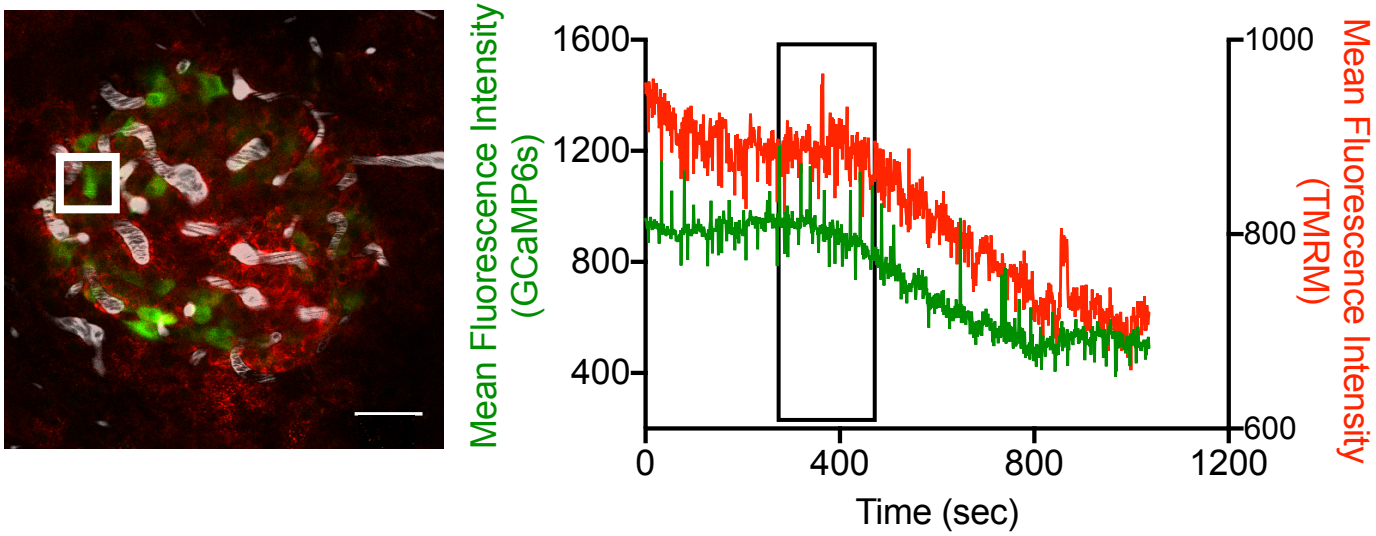
Mean Fluorescence Intensity (GCaMP6s)
1600
1200
800
400
Mean Fluorescence Intensity (TMRM)
1000
800
600
0
400
800
1200
Time (sec)

C

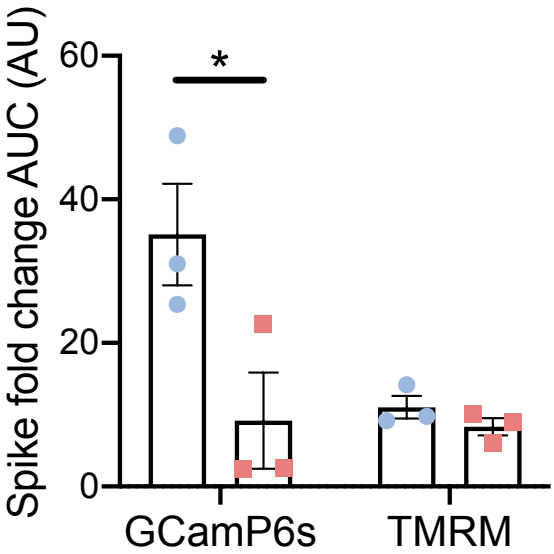
Spike fold change AUC (AU)
60
40
20
0
*
GCamP6s
TMRM

Fig.7

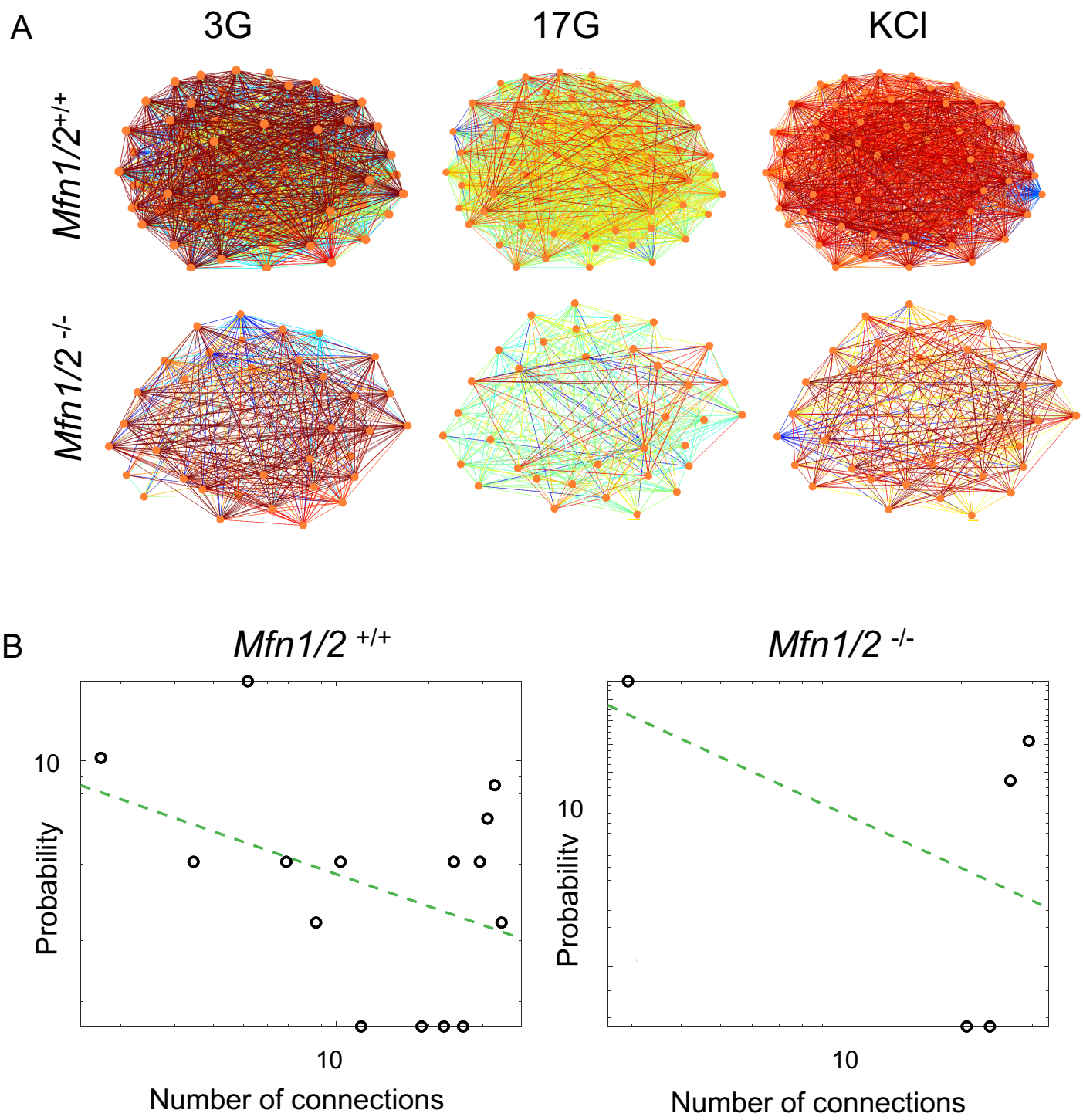
A
3G
17G
KCl
Mfn1/2+/+
Mfn1/2 -/-
B
Mfn1/2 +/+
Mfn1/2 -/-
10
Probability
10
Number of connections
10
Probability
10
Number of connections

Suppl. Fig.1

ESM Tables

ESM Table 1

Mfn1	F-TGGTAATCTTTAGCGGTGCTC
	R-GGAGGACTTTATCCCACAGC
Mfn2	F-TTTGGAAGTAGGCAGTCTCCA
	R-CAGGCAGCACTGAAAAGAGA

Sequence of primers used for genotyping *Mfn1* and *Mfn2* flox (F: forward, R: reverse).

ESM Table 2

Mfn1	F-GCATTTTTTGGCAGGACAAGTAG
	R-GGAGGACTTTATCCCACAGCAT
Mfn2	F-AGAAGAGTGTCAAGACTGTGAACCA
	R-GCTGCCTGCATGCAACTG
β-actin	F-CGAGTCGCGTCCACCC
	R-CATCCATGGCGAACTGGTG

List of primers used for qRT-PCR amplification (F: forward, R: reverse).